LRP 409/90 July 1990

TRANSPORT STUDIES FOR IGNITION EXPERIMENTS

A. Nocentini and C. G. Schultz

LRP 409/90 July 1990

TRANSPORT STUDIES for IGNITION EXPERIMENTS

Aldo Nocentini†, *Göran Schultz*‡*

†The NET Team

c/o Max-Planck-Institut für Plasmaphysik

Boltzmannstr. 2, D-8046 Garching (FRG)

‡Centre de Recherches en Physique des Plasmas

Association Euratom – Confédération Suisse

Ecole Polytechnique Fédérale de Lausanne

21 Av. des Bains, CH-1007 Lausanne, Switzerland

Abstract: The results of a predictive study of plasma energy confinement in IGNITOR, performed with a $1\frac{1}{2}$-D transport code and the Tang and Redi transport model, are reported. For comparison, performance predictions for NET adopting similar assumptions on plasma transport are also presented.

**Present address:* ERNE, Turun Yliopisto, Tykistökatu 4, 20520 Turku, Finland

1. Introduction

Tokamak fusion reactors are anticipated to require a major radius of the torus of the order of several meters, an aspect ratio of the order of 3, and a medium magnetic field (of the order of 5 Tesla on the magnetic axis, the field magnitude being limited by technological considerations).

Recently, a relatively small-size (major radius of the order of 1 meter, aspect ratio of the order of 3), high field (exceeding 10 Tesla on the magnetic axis) tokamak experiment (IGNITOR) was proposed /1/ to investigate the physics of ignition and fusion α-particles.

To assess the possible performance of this machine, a numerical analysis has been performed with the $1\frac{1}{2}$-D transport code JETTO /2/, using the transport model originally proposed by Tang and Redi /3,4/. Two "IGNITOR reference cases", with respectively 11 and 13 Tesla on the magnetic axis corresponding to two different designs, have been considered, and a sensitivity analysis of their performance has been done. Then, to investigate the influence of size on the performance, the same model used to simulate the IGNITOR discharges has also been applied to a NET-like plasma. For this, parameters corresponding to "NET II - 25 MA" /5/ have been adopted. Note that due to the differences between IGNITOR and NET (without/with additional heating, just to mention the most evident one) the comparison is not at all straightforward (for instance, the ratio of the α-power to the Ohmic power is a basic parameter for IGNITOR performance, while it is not for NET). Moreover, the physics is different in the two machines (L-/H-mode, just to mention the difference most relevant to transport), so that the use of the same transport model is questionable. Therefore, these simulations refer to a "NET-like" plasma with a physics similar to that of IGNITOR, rather than the actual NET. Finally, independently of the comparison with IGNITOR, we have performed some simulations of the actual NET II - 25 MA machine, taking

fully into account the NET operation scenario.

In section 2 the transport model is described in detail. In section 3 the results of the IGNITOR simulations are presented and discussed. In section 4 the results of the simulations of the NET-like plasma are presented and discussed, in particular in view of the results of the preceding section. In section 5 the results of the simulations of the NET II - 25 MA machine are presented and discussed. Section 6 is devoted to the conclusions.

2. The Transport Model

The Tang and Redi (TR) transport model /3,4/ has been used, in the form reported in /6/, with an added 20% reduction of the coefficients of the anomalous part of the heat conductivities. The coefficients reported in /6/ were in fact calibrated on TFTR results, /4/, and a 20% reduction was recently suggested to better reproduce global results of FT discharges /7/. In the TR model the electron heat conductivity is anomalous, while the ion heat conductivity is given by the sum of the neoclassical contribution /8/ and an anomalous contribution. The TR transport model is a "profile consistent" model in which the overall magnitude of the anomalous part of the heat transport coefficients is determined on the basis of a study of microinstabilities (trapped electrons drift modes and toroidal ion temperature gradient, "η_i ", modes).

The anomalous part of the heat transport coefficients which we use reads

$$\chi_s^{anom}(r)[cm^2/s] = 0.8\ F_s(r)\ \chi_{s,0}, \tag{1}$$

where $s = e, i$ for electrons and ions, respectively, r is a flux surface label ($\propto \sqrt{\Phi/\pi B_0}$, where Φ denotes the toroidal flux and $B_0[T]$ the toroidal magnetic field on the magnetic axis) normalized to 1 at the outermost magnetic surface (the

"edge"),

$$F_s(r) = \frac{\{1 - e^{-\alpha}\} e^{\frac{2}{3}\alpha r^2} p_s(r)}{\{n_s(r)/n_s(0)\} r^2 p_s(1)}, \tag{2}$$

$\alpha = q(1) + 0.5$, $q(1)$ denotes the safety factor at the edge, $p_s(r)[\mathrm{MW}]$ denotes the total power source on the s-th species within the magnetic surface whose label is r, the number density of the s-th species is denoted by $n_s(r)[10^{20} m^{-3}]$,

$$\chi_{e,0} = 4.3 \cdot 10^3 \frac{(1 + 0.25\gamma)\{p_e(1)\}^{0.8}}{n_e(0) R_0^{1.2} a^{0.1} Z_{eff}^{0.2} B_0^{0.4} \{q(1)\}^{0.9}} \qquad \text{for} \quad \nu_e* \geq 0.2, \tag{3}$$

and

$$\chi_{e,0} = 6.0 \cdot 10^3 \frac{\{p_e(1)\}^{0.6}}{n_e(0)^{0.6} \{B_0 R_0 q(1)\}^{0.8} a^{0.2}} \qquad \text{for} \quad \nu_e* < 0.2, \tag{4}$$

γ is the steepness parameter for a parabola approximating the density profile (it is determined by imposing that the number density $\hat{n}(r) = n_e(0)[1 - r^2]^\gamma$ gives the correct total number of electrons), $R_0[m]$ and $a[m]$ denote, respectively, the major and minor radii of the torus (the minor radius being defined as the square root of the ratio of the toroidal flux enclosed by the plasma and the product of π times the toroidal magnetic field), Z_{eff} denotes the effective value of Z, the electron collisionality

$$\nu_e* = \frac{\sqrt{2} R_0 B_0}{B_{\vartheta,0} v_{th,e} \tau_e \sqrt{\varepsilon}}, \tag{5}$$

is calculated on the $q = 1.5$ magnetic surface ($B_{\vartheta,0}$, $v_{th,e}$, ε and τ_e denote, respectively, the magnetic surface–averaged poloidal magnetic field, the electron thermal speed $\sqrt{2T_e/m_e}$, the inverse aspect ratio of the magnetic surface, and the electron

collision time $\tau_e = 3\sqrt{m_e}T_e^{3/2}/4\sqrt{2\pi}e^4 N_e \Lambda_e$, where Λ_e is the Landau logarithm),

$$\chi_{i,0} = 5.0 \cdot 10^3 \frac{\{p_i(1)\}^{0.6}}{n_i(0)^{0.6}\{B_0 R_0 q(1)\}^{0.8} a^{0.2}} \qquad \text{for} \quad \eta_i \geq 1.5, \tag{6}$$

and

$$\chi_{i,0} = 0, \qquad \text{for} \quad \eta_i < 1.5, \tag{7}$$

where η_i is the maximum value of $d(\ln\ T_i)/d(\ln\ n_i)$ in the region between the magnetic surfaces $q = 1$ and $q = 2$.

In most simulations the electron and ion heat conductivities have been assumed to jump discontinuously, at the thresholds $\nu_e* = 0.2$ and $\eta_i = 1.5$ respectively, from the value they have on one side of the threshold to the value they have on the other side. This should be regarded as a trick to easily identify the time instants at which the thresholds are crossed, in the plots. At these instants, sudden variations appear in the values of some quantities, like the energy replacement time, and in the rate of variation of other quantities, like the central temperatures. The introduction of smooth transitions of the values of the heat conductivities has only the effect of smoothing these variations in time. Of course, it gives also the possibility of reaching steady states in which ν_e* and/or η_i remain close to their threshold values. In this case, the coefficients of the anomalous parts of the electron and/or ion heat conductivities, $\chi_{e,0}$ and/or $\chi_{i,0}$, have values which are intermediate between equations (3) and (4) and/or equations (6) and (7).

To avoid too low a value of the safety factor on the magnetic axis, in most simulations the safety factor was just constrained to remain above a given value ($q_0 = 0.7$). From a formal point of view, this is equivalent to assuming the presence of an "electromotive" (i.e. noninductive) electric field opposing the current (inside the magnetic surface where $q = q_0$). From a physical point of view, this is

equivalent to assuming the existence of some kind of instability which, as soon as q decreases below q_0, grows and redistributes the electric current so that q returns to its limiting value q_0, while the other transport properties (of particles and heat) of the plasma remain unaffected. The main consequence of this model (already used in /7/) is the reduction of the Ohmic heating in the central region of the plasma column (inside the $q = q_0$ surface), and an increase in the outer region. A sensitivity analysis (see §3) has shown that the influence of the choice of the value q_0 on the performance of the machine is negligible.

As far as particle transport is concerned, the Alcator-INTOR model has been chosen for the transport coefficient, and an inward pinch has been included, as proposed in /9/, the coefficients being adjusted in order to get the desired rate of particle pinching.

In the heat balance equation, the factor 3/2 has been used for the energy convection term.

It is worthwhile to mention some general consequences of the transport model, which can immediately be concluded from the form of the dependence of $\chi_{e,0}$ and $\chi_{i,0}$ on the plasma parameters. Firstly, high density plasmas are favoured, and plasmas with peaked density profiles are even more favoured, because the heat transport coefficients decrease as the density on the magnetic axis increases (note that the factor $1 + 0.25\gamma$ in the numerator on the right hand side of equation (3) cannot compensate for the $n_e(0)$ in the denominator). Secondly, the confinement degradation with power is extremely strong at relatively high collisionalities (i.e. at relatively low powers). At low collisionalities (i.e. at relatively high powers) it is less strong, although still larger than in most of the accepted scaling laws. Finally, by comparing the expressions of the known power scaling laws for tokamak energy confinement time (τ_E) with the coefficients of the Tang and Redi model, for constant values of aspect ratio and safety factor at the edge (which implies

constant values of aB_0/I), this model turns out to generally have a more favourable dependence on density (n) and size (L) and a less favourable dependence on power (p), current (I) and magnetic field. For example, $\tau_E \propto L^{2.35} n^{0.1} B_0^{1.25} p^{-0.5}$ for the ITER scaling law /10/, while $\tau_E \propto L^{3.4} n^{1.0} B_0^{0.6} p^{-0.8}$ and $\propto L^{3.0} n^{0.6} B_0^{1.0} p^{-0.6}$ for $\nu_e* > 0.2$ and < 0.2 respectively, in the case of the Tang and Redi model.

The predictions of the TR model were compared with experimental results for a number of devices. The results of a detailed comparison with JET (Ohmic and L-mode) shots are reported in /11/. The general conclusion is that the TR model tends to overestimate (by up to 50%) the temperatures (and, therefore, the energy confinement time) of Ohmic discharges. For discharges with additional heating the discrepancy tends to become smaller as the amount of additional heating increases. It should be mentioned that this overestimation was also found for the FT discharges we considered. As an example, in fig. 1 the results are reported of the simulation of the ASDEX shot #17529 /12/ at the instant $t = 1.05\,\mathrm{sec}$, i.e. during the steady state obtained in the Ohmic phase. The measured loop voltage was $V_L = 1.25$ and the energy confinement time $\tau_E = 0.087$. The simulation was done with diffusion coefficients larger (by 25%) than those used in the IGNITOR simulations, i.e. with the coefficient 1.0 replacing the 0.8 in equation (1). Also, a simple sawtooth model was used. The density profile was kept fixed, equal to the experimental one.

As far as the model for alpha particle production and energy deposition is concerned, it has been assumed that the alpha particles created by the D-T reaction release their energy locally in space (i.e. no alpha particle transport is considered) and progressively in time (accordingly to their slowing-down process). The dilution of the D-T plasma due to the production of alpha particles has not been taken into account.

3. Simulations of IGNITOR

Two main IGNITOR configurations have been considered, which will be referred to in the following as "high field" ($B = 13.12\,\mathrm{T}$, $I = 12\,\mathrm{MA}$) and "low field" ($B = 11.11\,\mathrm{T}$, $I = 10\,\mathrm{MA}$). In both cases, the geometrical parameters are $R_0 = 1.175\,\mathrm{m}$ and $a = 0.6\,\mathrm{m}$, and the safety factor at the edge is $q(a) = 2.8$. For each case we have a "reference run", evolving for 7 seconds (from $t = 0$ to $t = 7\,\mathrm{sec}$) from given initial conditions (see below). The equilibrium is calculated at $t = 0$ and the shape of the magnetic surfaces is kept fixed during the run. The plasma composition is deuterium, tritium and two impurity species, carbon and oxygen. The value of the recycling factor is 1 for all species, and deuterium and tritium are assumed to have the same density. The edge temperature $T_{edge}(t)$ (for both ions and electrons) increases linearly during the first second from a low value to $T_{edge}(\infty) = 600\,\mathrm{eV}$ and remains constant for $t \geq 1\,\mathrm{sec}$.

For each reference run a sensitivity study has been performed with respect to changes in various parameters and conditions. This study was rather complete for the "low field reference case". With some exceptions, all the runs simulate the discharge for 7 seconds. The runs are presented below and their summary in the Tables. A suitable figure of merit for the performance of the various runs is the ratio $\Re$ of the alpha power deposited in the plasma to the Ohmic power. In the tables we give the instants t_1, t_2, t_4, t_{10} at which $\Re = 1,\ 2,\ 4,\ 10$, respectively, is reached and the value of $\Re$ at $t = 7\,\mathrm{sec}$. Moreover, we give the sign of the first and second derivatives (P'_α and P''_α respectively) of the α-power. They give an idea of the behaviour of the discharge for $t > 7\,\mathrm{sec}$ (a tendency towards a steady state is displayed by the combinations [+,−] and [−,+]; that a steady state is already reached is displayed by the combination [0,0]; a thermal instability (ignition) is displayed by the combination [+,+]; a thermal collapse is displayed by the combination [−, −]).

3.1 The low field reference run

The low field reference run (referred to as LF0 in the following), the essentials of which can be seen in fig. 2 and Table I, is characterized by the fact that it tends to a steady state in which the alpha power dominates the Ohmic power ($\Re \approx 4$) and the ion heat transport is neoclassical, because η_i remains below threshold during the whole discharge. The existence of such steady states is made possible by the strong dependence of the heat conductivities on power. The initial density profiles are parabolic squared, with central ion density 1.5×10^{21} m^{-3}, and the initial temperature profiles are parabolic, with central temperatures 4.6 keV for the electrons and 3.9 keV for the ions. The central densities of carbon and oxygen are 6×10^{18} m^{-3} and 6×10^{17} m^{-3}, respectively, leading to a Z_{eff} of 1.20. The minimum q is forced to remain above $q_0 = 0.7$, which impedes accumulation of the current in the center and results, at the end of the run, in a centrally rather flat, even slightly hollow current profile, the flat region (where q takes on its central value) extending almost up to half radius. The electron temperature profile changes within one second from its initial parabolic-squared shape into a bell-shape. The central temperature then climbs steadily from the initial value of 2.95 keV to a final value of 10 keV. The Ohmic power density, fig. 2(g), is characteristically peaked off-axis. In the central region, its dependence reflects the flat current density profile in the presence of a centrally peaked electrical conductivity (as a consequence of the electron temperature profile and the trapped particles effect). Here, the coefficient of the anomalous inward pinch ($\alpha_{inw} = 3.0$) is chosen in such a way that the "peakness factor" of the density ($n_e(0)/\bar{n}_e$, where $\bar{n}_e$ is the volume average of the electron density) remains almost constant (changing from 2.7 at $t = 0$ to 2.9 at $t = 7$) during the discharge. Actually, fig. 2(d), the density profile remains rather steady. The loop-voltage shown in fig. 2(c) represents the averaged Ohmic value. It comes down steadily from an initial 1.6 V to a final

0.7 V at 7 seconds. For this discharge, the energy replacement time τ_E, fig. 2(b), has a peak value of 460 ms at 1.5 seconds and drops to 350 ms at 7 seconds. The alpha-power bypasses twice Ohmic power at 4 seconds, fig. 2(a).

3.2 Sensitivity analysis of the low field case

Firstly, the sensitivity of the performance of the reference run to the relatively high initial temperature was investigated. By halving the value of the pressure, the initial temperatures of the reference run were brought down to half their values (LF1: $T_e(0) = 2.3\,\mathrm{keV}$, $T_i(0) = 2.0\,\mathrm{keV}$). In this case, for the initial 2 seconds studied, the alpha power increased in the same fashion as for the reference case, though at a slightly lower rate ($\Re = 1$ was obtained at $t = 2.3\,\mathrm{sec}$). This is a consequence of the fact that, starting from a lower ion temperature, the α-particle source is initially smaller and more time is therefore needed to build up a significant α-particle concentration and, hence, the associated power source.

The effect of sawteeth is very bad for the performance of the machine. Sawtooth crashes were simulated by increasing transport in the central region by including a Bohm-like term or by allowing for density and temperature flattenings inside the magnetic surface $q = 1$ every time the value of q on the axis went below 0.8. We have allowed in LF2a as little as 10% of Bohm diffusion, imposed below $q = 0.8$ – in other words between 0.7 and 0.8 which is half the radius and one quarter of the volume, and see a value of $\Re$ below 0.5 despite good confinement, τ_E of 470 ms. In LF2b the lower bound to q_0 ($q_0 = 0.7$) was taken out, so that current penetration was classical (a central q value of 0.35 was obtained at $t = 7\,\mathrm{sec}$), and 10% of Bohm diffusion was allowed for $q < 0.7$, leading to a similar result ($\Re = 0.42$ at $t = 7\,\mathrm{sec}$), in spite of having recalculated the equilibrium at $t = 0.5,\ 1.0,\ 2.0$ and 4.0, which tends to improve (see below) the performance of the discharge. In LF2c, where the reconnection model was used, a sawtooth

period $\tau_{st} \approx 0.1$ sec was found and a low-$\Re$ ($\Re = 0.17$) "steady state" was rapidly reached.

Raising the value of the anomalous electron heat conductivity by changing the coefficient of equation (1) from 0.8 to the standard value of 1.0 (run LF3) is fatal: the value of $\Re$ at $t = 7$ sec is 0.04. Of course, only the electron heat conductivity is relevant here, because the ion heat conductivity remains in any case neoclassical.

In LF4 and LF4a the effect of a larger impurity content was studied. Doubling the carbon and oxygen central densities increased Z_{eff} to 1.33. In this case (LF4), $\Re$ increases much slower in time, with respect to LF0, reaching 1 only after 3 seconds and tending asymptotically to a relatively low value ($\Re = 1.54$ at $t = 7$ sec). Tripling the impurity content (LF4a) leads to $Z_{eff} = 1.46$ and brings the value of $\Re$ below 1.

Lowering the primary central densities by 20% (to 1.2×10^{21} m^{-3} (LF5)) decreases substantially $\Re$ (only 1.6 at $t = 7$ sec), much more than expected from the small related increase of Z_{eff}. Note that the energy confinement time is in this case, at the end of the shot, 0.40 sec. Note also that with less density the discharge reaches its stationary phase in a shorter time, so that its behaviour seems to be better, if only the first phase is looked at. This is due to two facts. Firstly, a lower initial density implies a higher initial temperature (because the initial pressure profile is kept fixed in our simulations). Secondly, in the initial phase, where Ohmic heating is the dominating heating mechanism, a lower density helps to increasing the heating rate of the plasma column. Of course, in the final phase the α-power source, which is proportional to the density squared, is more important in determining the temperature. The shot LF5a, where the central value of the density was kept fixed while the density profile was chosen parabolic instead of parabolic squared (with, hence, a substantial increase of average density), confirms this interpretation: the too high value of the density impedes heating in the early

phase, and $\Re$ increases slowly to 0.24 at $t = 7\,\mathrm{sec}$.

Changing the fraction of deuterium from the initial 50% to 70% (LF6) has also a strong impact on the performance of the discharge, in spite of the moderate decrease (by 16% only) of the α-power source. In this case, $\Re$ reaches 1.12 at $t = 7\,\mathrm{sec}$.

Lowering the current in the reference run to 9 MA (LF7) does also lead to a lower performance: $\Re = 1$ is achieved at 3.9 seconds and $\Re = 1.1$ at $t = 7\,\mathrm{sec}$. Decreasing the density by 20% (LF7a) confirms that a lower density allows to reach the steady state in a shorter time, but at a lower value of $\Re$. This is clearly shown by the comparison of the values of $\Re$ at $t = 0.1,\ 1.0,\ 2.0,\ 7.0\,\mathrm{sec}$ for the two shots. We get 0.17, 0.24, 0.50, 1.1 in LF7 and 0.29, 0.57, 0.98, 0.97 in LF7a.

Lowering the value of the edge temperature leads to a lower performance, until a kind of threshold value is reached, below which the discharge ends in a very low-temperature steady state, like that one which is found by increasing the transport coefficients by 25%. This is shown by LF8a, where the edge temperature T_{edge} for $t \geq 1\,\mathrm{sec}$ was lowered to $T_{edge}(\infty) = 400\,\mathrm{eV}$ and $\Re = 2.1$ was reached at $t = 7\,\mathrm{sec}$, and LF8b, where $T_{edge}(\infty) = 300\,\mathrm{eV}$ and $\Re = 0.05$ is reached. No attempt has been made to determine the parameter dependence of the threshold temperature. This should actually be regarded as an extremely important item, because the plasma is assumed to be extremely clean and it is difficult to reconcile this requirement with a high temperature in front of the edge.

If the edge temperature is raised, the performance of the discharge increases. In shot LF8c $T_{edge}(t)$ increases linearly in time from 160 eV at $t = 0$ to 1200 eV at $t = 2\,\mathrm{sec}$ and remains constant for $t > 2\,\mathrm{sec}$. This leads to $\Re = 113$ at $t = 6\,\mathrm{sec}$, where the α-power (215 MW) is still increasing linearly in time at a rate of almost 90 MW per second, although its second derivative starts to become negative. This shows that, if the edge temperature is high enough, ignition cases

can easily be found. Of course, they can also be found if the edge temperature is not increased but the values of the heat transport coefficients in front of the edge are decreased below what is foreseen by the TR model. This leads in fact to the formation of a temperature pedestal in front of the edge, which has the same effect as increasing the edge temperature. To this effect can probably be ascribed the difference between our results and those, much more favorable to IGNITOR, presented in /7/, where the transport coefficients in front of the edge were limited by a Bohm-like expression.

The effect of increasing the anomalous particle pinch has a favourable effect on the discharge, because it tends to increase the α-power source progressively in time, without affecting the discharge too much in the initial phase, when too high a density would impede Ohmic heating from attaining a high enough temperature. This effect can be seen in LF9, where the reduction by 33% of α_{inw} leads to a reduction of $\Re$ by 43%. Recalculating the equilibrium during the time evolution of the discharge has the same favourable effect, because of the diamagnetic pinch related to the current penetration. In LF0r, the shot LF0 was repeated by recalculating the equilibrium at $t = 0.5,\ 1.0,\ 2.0$, and 4.0 sec, with a strong improvement of the performance of the discharge.

The effectiveness of a somewhat lower density coupled to a strong particle pinch and recalculation of the equilibrium is exhibited by the three shots LFa, LFb and LFc (Table II). They are similar to LF0, but for the value of $T_{edge}(\infty)$, which is 400 instead of 600, the value of the central ion density, which is 20% lower, and the value of α_{inw}, which is 2, 3 and 10, respectively, in the three shots. In LFa the boundary temperature is clearly below threshold. The same boundary temperature is clearly above threshold for shot LFb, the change being due to the higher value of α_{inw}. This shot, compared to LF8a, shows the accelerating effect of a lower density on the performance of the discharge. Eventually, shot LFc exhibits,

with its high performance, the fundamental importance of dynamic peaking of the density. In this shot, the final value (at $t = 7\,\mathrm{sec}$) of the peaking factor of the density is 5.3 (initial value 2.5).

Another series of shots at increasing strength of the anomalous particle pinch is LFd to LFg (see Table II). Here the initial density profile is parabolic (the initial value of the peaking factor is 2) and the average particle density is slightly larger than in LF0 ($\bar{n}_e = 6.2 \times 10^{20} m^{-3}$). The first shot ends in a low-$\Re$ steady state. The other three shots show a very good performance and, at the same time, a peculiar behaviour. They seem to smoothly evolve into a low-$\Re$ steady state (this is particularly evident for the shots LFe and LFf), when, suddenly, the α-power starts to increase, the energy confinement time increases, the transport losses decrease. From a detailed analysis, it is possible to see that the precursor of this "explosion" is due to an increase of the electron temperature just in front of the edge. This implies that the energy input to the electrons decreases there, because they loose more power to the ions. As a consequence of the transport model adopted, the (anomalous) electron heat conductivity in front of the edge decreases, so that the electron energy loss through the conduction channel decreases. If the ion heat conductivity were also anomalous, the ion energy loss through the conduction channel would increase, due to the increase of the power they receive, compensating the reduced electron losses. But in our case the η_i threshold is never reached, the ions are neoclassical and, therefore, the associated heat losses remain unchanged. Hence, a kind of thermal instability develops as a consequence of the thermal insulation of the edge. In Table II, for the first shot, the peaking factor at the end of the run is shown. For the other three shots, in which the α-power starts to increase at a well-defined time instant, this is shown together with the value of the peaking factor at that moment. By looking at the values of the central temperature and τ_E at these instants, it is possible to deduce the rough rule that,

in order to be able to start towards ignition or atleast towards a high-$\Re$ steady state, the temperature on axis should be of the order of 5 keV and, simultaneously, the energy confinement time larger than 0.4 sec.

Shot LFg is a high-performance shot with still a reasonable, although large, density peaking (3.3 at $t = 7$ sec). A sensitivity analysis was also performed starting from this shot, to see if the negative influence of some of the variations could be mitigated by the higher performance of the starting point. The results are presented in TABLE III, which is self-explanatory. With respect to the sensitivity analysis of LF0, two additional cases are considered here. Firstly, to see the influence of the presence of anomalous ion heat conduction, the η_i threshold was arbitrarily lowered (to 0.6 in LFg1a and to 0.4 in LFg1b). In LFg1b the ion heat conductivity is always anomalous, and the discharge tends smoothly to a low-$\Re$ steady state where the heat loss due to conductivity is 60% on the electron channel and 40% on the ion channel. In LFg1a the discharge is near threshold, so that the anomalous ion heat conductivity is not always on. As a consequence, the shot shows phases of "good behaviour", during which the ion heat conductivity is neoclassical and the plasma temperature increases, and phases in which, having the ion temperature peaked enough so that the threshold is reached, the ion heat conductivity is anomalous and the temperature drops. Secondly, the relatively weak influence of the value of q_0 is shown by LFg6a and LFg6b. Shot LFg6c has a similar behaviour up to $t \approx 5.7$ sec, where the rising of the tempeature is suddenly stopped, and the performance starts to worsen. This is not directly due to the change of q_0, but to the fact that it causes the reaching of the η_i threshold at $t \approx 5.7$ sec and the turning on of anomalous ion heat conductivity.

3.3 The high field reference run

The high field reference run (referred to as HF0 in the following), presented

in Table IV and in fig. 4, differs slightly from the low field reference run LF0 in having the anomalous inward pinch initially set to α_{inw}= 2.5 and the central ion density initialized as 1.2×10^{21} m^{-3}. Like the low field reference run, it tends to a steady state in which the alpha power is dominating the discharge. The lower initial density is reflected as slightly higher initial central temperatures 5.5 keV for the electrons and 4.7 keV for the ions, and with impurity densities the same, the resulting Z_{eff} becomes 1.25.

During the discharge, the density profile remains essentially unchanged after the first second, while the central electron and ion temperatures rise steadily to the final values of 17.5 keV and 16.5 keV. The current profile reaches its characteristic flat character up to half the radius in 1.5 seconds. The energy replacement time τ_E has a peak value of 420 ms at 1 s and drops to 240 ms from 4 s onwards. As for $\Re$, the alpha power bypasses twice Ohmic power at 1.3 s, four times at 1.8 s and ten times Ohmic power at 3.7 s.

3.4 Sensitivity analysis of the high field case

Sensitivity tests mirroring those of the low field reference run were carried out. The first modification of the reference run, HF0r, recalculating the equilibrium at t = 0.5, 1.0, 2.0, 4.0 seconds, shows the sharp discontinuities in the transport properties as the equilibrium is recalculated, resulting in fairly small changes in the physical parameters, as well as the change at 2.2 seconds when the η_i criterion has first been met, resulting in a qualitatively changed discharge. Up to that instant the discharge shows a behaviour very similar to HF0 and to the behaviour found for the low field reference case (generally, recalculating the equilibrium improves the alpha power), from that instant onwards its performance drops and the discharge tends to a much lower-$\Re$ steady state. The physical parameters ($< T_e >$, $< T_i >$, τ_E, etc.) show abrupt variations in their rates of change, which are clearly related

to the abrupt onset of the anomalous ion heat conductivity.

Simulating the sawteeth with 10% of Bohm diffusion imposed below $q = 0.8$, HF1, resulted in a quenched alphapower, reaching a peak $\Re = 2.6$ at 1.8 seconds, but then falling off to 1.6 at 7 seconds. The energy replacement time τ_E rises to a peak of 420 ms at 1.2 seconds, drops to a minimum of 350 ms at 2.2 seconds and has a final value of 380 ms at 7 seconds, indicating that we have a marginal case for the combination of parameters and transport model chosen.

Raising the value of the anomalous electron heat conductivity to the standard value, HF2, is as fatal here as it was for the low field case: a steady state with alpha power equal to Ohmic power resulted.

Increasing the impurity content by doubling the central densities of carbon and oxygen, HF3, gave a $Z_{eff} = 1.43$ but only a quantitative decrease of the ignition rate: by the end of the discharge $\Re$ was 7.3. Increasing the deuterium ratio to 70%, HF4, is similar: a final steady-state $\Re$ of 3.5 is reached at 7 seconds.

A more interesting result was reached by lowering the anomalous inward pinch α_{inw} to 2.0, HF5. The discharge starts off like the high field reference run, but $\Re$ reaches a peak of 8.5 at 4.2 seconds and falls off as if quenching to 3.6 at 7 seconds. A closer examination of the discharge reveals that the anomalous ion transport has been triggered, increasing the losses through the ion channel by almost a decade. The high field reference run itself does not trigger anomalous ion transport.

The physics for ion transport was given in equations (6) – (7), but the formula actually used is a smoothed version

$$\chi_{i,0} = \chi_{i,00} H(\eta_i^m - \eta_i^{crit})$$

where $\chi_{i,00}$ is given by equation (6), η_i^m is the maximum value of $d(\ln\ T_i)/d(\ln\ n_i)$ in the region between the magnetic surfaces $q = 1$ and $q = 2$, and $H(x) = (1 + \tanh(xz))/2$.

A set of runs were carried out to study sensitivity to this triggering with respect to smoothing (z) and varying the η_i threshold ($\eta_i^{crit} = 1.5$ and $z = 50$ in the reference run).

Without recalculating the equilibrium, varying z to 4, HF6b1, and 2, HF6b2, shows a degrading of performance with respect to our reference run HF0, due to the fact that although the discharge remains below threshold, χ_i has a small anomalous part due to the presence of the smooth transition.

Varying z to 20, HF6a1, and 5, HF6a2, while recalculating the equilibrium shows essentially the reference case HF0 and not HF0r (recalculated equilibrium), indicating that such an insignificant modification is enough to change the global transport picture by making the difference between neoclassical and anomalous ion heat conductivity. For the latter case, HF6a2, $\Re$ remains below 10 (8.1 at 7 seconds) and the transport properties are smooth.

3.5 Conclusions

From the previously described IGNITOR simulations using the Tang and Redi model, the conclusion can be drawn that many conditions have to be simultaneously fulfilled to obtain IGNITOR discharges in which, at least at the end of the discharge (we recall here that the flat-top time of IGNITOR is of the order of 4 seconds), α-particle heating becomes the dominant heating mechanism. These are the following:

(i) ion heat conductivity losses must be at the neoclassical level,

(ii) neither sawteeth activity nor other types of enhanced transport are present in the center,

(iii) a high temperature is present at the plasma edge,

(iv) a very low impurity concentration is ensured,

(v) a high peaking of the density must be obtained.

These conditions were obtained with the Tang and Redi transport model adopting a reduced coefficient (0.8) in front of the anomalous heat conductivities (smaller than required to simulate most tokamak experiments). This prescription could be referred to as condition (vi).

Within the framework of the model (the aforementioned prescription included), conditions (i) and (ii) are "hard", in the sense that the introduction of anomalous ion heat losses or sawteeth activity degrades confinement to such an extent that it cannot be compensated in any way, not even by making conditions (iii) to (v) as far as possible more restrictive. If conditions (i) and (ii) (and vi) are fulfilled, a possible quantification of conditions (iii) to (v) is the following: $T_{edge} > 500eV$, $Z_{eff} < 1.3$ and density peaking factor increasing from 2 to 3 during 4 seconds. Actually, it is difficult to reconcile the first two requirements, and the third one requires a very careful control of the plasma density profile, which should provide peaking without cooling. Of course, some conditions can be relaxed if other ones are simultaneously made more stringent. For example, increasing the peaking rate of the density allows to decrease the edge temperature, as shown by shots LFa to LFc.

4. Simulations of a NET-like plasma

In order to examine the effect of size on the performance, the same transport model used for the IGNITOR simulations was also used for a few simulations of a NET-like plasma. To this aim, the parameters of "NET II - 25 MA" /5/were used. These are $B = 6.0\,\mathrm{T}$, $I = 25\,\mathrm{MA}$, $R_0 = 6.3\,\mathrm{m}$, $a = 3.041\,\mathrm{m}$ (corresponding to an actual horizontal minor radius of 2.05 m and an elongation of 2.2). The magnetic surfaces were assumed in the simulations to have elliptic, concentric cross sections, resulting in a safety factor of 2.5 at the edge. The average electron density was $0.92 \times 10^{20} m^{-3}$. As in the IGNITOR simulations, a 50-50 DT mixture in the

presence of carbon and oxygen impurities was considered, with a recycling factor 1 for all the species. The edge temperature (for both ions and electrons) was assumed to be constant, 40 eV, in the initial, 5-seconds long Ohmic phase (from $t = -5$ sec to $t = 0$ sec), to increase linearly in time to $T_{edge}(\infty)$ in the following second, during which the additional heating power increased linearly from zero to its maximum value, and then to remain constant. In this way the "initial" state, i.e. the state at the beginning of the additional heating phase (at $t = 0$ sec), was a self-consistent Ohmic equilibrium. The main differences, with respect to the IGNITOR simulations, was a higher impurity content ($\bar{Z}_{eff} = 1.9$ in the reference run for NET) and a parabolic profile for the initial density, with the strength of the inward pinch chosen in such a way that the peaking factor for the density remained almost constant (≈ 2) during the simulations.

In the following subsections we describe the NET reference run and the results of a sensitivity analysis for it.

The discharges were let to evolve for 10 seconds or more during the additional heating phase and the value of $\Re$ at $t = 10$ sec (i.e. after 9 seconds of additional heating at full power) is usually reported in TABLE V, which summarizes the results. This was done to be able to compare analogous quantities for both NET and IGNITOR. In the case of NET, due to the presence of the additional heating, the ratio of the α-particle power to the additional power is, during the time the additional heating is on, the better performance parameter.

In the case of NET, it is interesting to consider also simulations in which the additional heating power is on for a limited time interval. Therefore, a number of discharges have been simulated in which the additional power increases linearly in time from zero to the full value over one second, remains constant for a given "heating time", and then decreases linearly in time from the full value to zero, again over one second.

4.1 The NET-like reference run

The NET-like reference run (referred to as NT0 in the following), the essentials of which can be seen in fig. 6 and in Table V, is the counterpart of the reference runs for IGNITOR.

We again stress the presence of a higher impurity content, obtained by assigning the amount of carbon and oxygen (in the ratio 5 to 1) needed to get $Z_{eff} = 1.9$ and the absence of any peaking of the initial (parabolic) density profile. To simulate the effect of the additional heating system, 88 MW of total (magic) power is assigned and equally distributed (50%-50%) to ions and electrons, with a parabolic power density profile.

The edge temperature for $t > 1$ sec is, as in the IGNITOR reference runs, $T_{edge}(\infty) = 600$ eV. The lower boundary of the safety factor, q_0, is also 0.7, but in the case of NET this boundary plays a negligible rôle, because the region where $q = 0.7$ is very small. The magnetic surface on which $q = 1$ is located at roughly half radius, while in the IGNITOR case it was at two thirds of the radius.

In order to compare the NET-like and the IGNITOR reference cases under the same conditions as far as the transport coefficients are concerned, in this run the ion heat conductivity was imposed to be neoclassical (for $t > 4.0$ sec).

Under the action of the additional heating, the plasma heats up and the α-power becomes equal to the additional power at $t = 7.1$ sec. At the end of the run ($t = 10$ sec), the α-power has reached a value of 225 MW and continues to increase at a rate of 40 MW per second, while the central temperatures (almost equal for both species) are larger than 20 keV, and increase at a rate of almost 3 keV per second.

The shot NT0a is identical to NT0 apart from the fact that the ion heat conductivity is set to be neoclassical at all times, and the additional heating time is 13 seconds (i.e., the additional power is on at its full value for 13 seconds).

The initial behaviour of this discharge is, of course, similar to that of NT0. After turning off the additional heating, the plasma tends smoothly to a high-$\Re$ steady state. The asymptotic value of the α-power is 486 MW, of the central electron and ion temperatures it is 33 and 38 keV, respectively. By increasing the heating time, higher-$\Re$ steady states are reached, the parameters of the steady state being essentially equal to the parameters reached by the plasma at the end of the heating phase, as if a region of "indifferent" equilibrium were reached by the plasma. Actually, an extremely slow time evolution (almost negligible on a 10 sec time scale) towards a common steady state can be seen in the longer runs.

The assumption of neoclassical ion heat conductivity could, perhaps, be justified for IGNITOR, but is questionable for NET. On the other hand, NET should work in the H-mode, not in the L-mode. Hence, a NET-like plasma should be better simulated by letting χ_i be anomalous and reducing the TR transport coefficients by a factor of the order of 2. These two corrections tend to compensate each other, as shown by shot NT0b, which differs from NT0 and NT0a in the ion heat transport, anomalous in NT0b, and in the heat diffusion coefficients, which in NT0b are reduced by 12.5% with respect to the IGNITOR runs, i.e. by 30% with respect to the standard values calibrated against L-mode TFTR shots by Redi et al. /4/. Moreover, in NT0b the heating time is 28 seconds and the additional power 44 MW. In this run, at the end of the additional heating pulse, the plasma goes into a high-$\Re$ steady-state in which $P_\alpha = 240$ MW.

In order to compare IGNITOR with NET more directly, the sensitivity analysis which follows has been done with respect to NT0 (neoclassical ion heat transport, L-mode).

4.2 Sensitivity analysis of the NET-like reference run

The sensitivity to the introduction of anomalous ion heat transport was exa-

mined in the shot NT1, where χ_i is anomalous all the time. This shot shows the tendency to go into a high-P_α steady state ($P_\alpha = 255\,\mathrm{MW}$ after 19 seconds of heating at full power, with $P'_\alpha = 8\,\mathrm{MW/sec}$, decreasing). By limiting the heating time, the α-particle power reaches a maximum at the end of the heating pulse, and then decreases again (see NT1b, NT1c, NT1d). With a 20 seconds heating pulse, P_α becomes again equal to P_{Ohm} at $t = 60\,\mathrm{sec}$.

The sensitivity of the NET-like reference run to a reduction of edge temperature (NT2), to the inclusion of Bohm diffusion in the central region of the discharge (NT3a to NT3e) and to a 50% increase of the coefficients of the anomalous heat conductivities (NT4) was also studied. The results are presented in Table V and show clearly that the NET-like reference run is much less sensitive than the IGNITOR reference runs to these modifications.

In Table V are also reported two cases in which the amount of additional power was reduced by 30%, Bohm diffusion was included inside the magnetic surface $q = 1$ and the length of the heating pulse was limited (NT5a and NT5b). Also in these cases the discharge tends, after the additional heating is shut off, to a steady state at high P_α.

4.3 Conclusions

From the simulations presented above it appears clearly that going from IGNITOR to NET parameters allows reaching ignition in a wide parameter range. In particular, density peaking is not required at all; Z_{eff} can be much higher, fully justifying the assumed values of the edge temperature; lower values of the edge temperature are actually allowed; a substantial degradation of confinement inside the $q = 1$ surface is also allowed. The condition which is to be maintained is that either the ion transport is neoclassical, or the numerical coefficient in front of the anomalous transport conductivities is reduced (from 0.8 to 0.7, see the next

section and fig. 13), or the temperature in front of the edge is larger (from 0.6 keV to a few keV, see the next section). This is not surprising, as a NET-like plasma cannot be expected to ignite in L-mode operation as described by a particularly unfavourable scaling of energy confinement time with heating power.

In the absence of a transport model specifically validated against H-mode discharges, H-mode operation is usually simulated by reducing the L-mode heat conductivities by a factor of the order of two. Alternatively, one could increase the edge temperature to simulate the formation of the temperature pedestal at the separatrix.

5. NET II - 25 MA modelling

In this section we present and discuss the results of some NET simulations made by taking into account, as far as possible, the peculiarities of the NET II - 25 MA scenario /5/.

The machine parameters were chosen as given in /5/and used in the preceding section ($B = 6.0\,\mathrm{T}$, $I = 25\,\mathrm{MA}$, $R_0 = 6.3\,\mathrm{m}$, $a = 3.041\,\mathrm{m}$, coming from a small minor radius of 2.05 m and an elongation of 2.2). The magnetic surfaces were approximated by tori with elliptic, concentric cross sections ($q(a) = 2.5$). The particle profiles were assumed to be fixed in time (particle transport and pinch were not included). A 50–50 DT mixture in the presence of carbon and oxygen as impurities was considered, with such concentration that $Z_{eff} = 1.9$. In the absence of a final decision on the additional heating method which will be chosen for NET, the additional power was assumed to be equally distributed between ions and electrons, with a parabolic deposition profile, and to be applied progressively, increasing linearly in time from zero to the full value during the first second of the simulation, remaining constant for a given time (the heating time), decreasing (linearly in time) during the following second and then remaining zero. The edge

temperature (for both ions and electrons) was assumed to increase linearly in time from 100 eV to 600 eV during the first second and then to remain constant. The initial temperature profiles were assumed to be parabolic, with central values of 3000 eV.

The electron and ion heat conductivities were taken according to the Tang and Redi model, with a reduction factor to represent H-mode operation. Note that in the following the reduction factor is given with respect to the full value of the Tang and Redi conductivities, which was calibrated against L-mode TFTR shots by Redi et al. /4/. Note also that the IGNITOR simulations presented in Section 3 used a reduction factor 0.8.

5.1 NET II - 25 MA simulations

The simulations show that, for the NET reference electron density of $\bar{n}_e = 0.9 \times 10^{20}\ \mathrm{m}^{-3}$, with square-root-of-parabolic profile, a reduction factor 0.6 (i.e. an enhanced confinement factor with respect to the L-mode equal to 1.67) is sufficient to get the desired performance, i.e. ignition is reached. This is shown in fig. 7(a), where the time behaviour of the powers is given for a case where 44 MW were applied for 20 seconds and a steady state with $P_\alpha = 240$ MW was reached (shot NETa). That the amount of additional power used can easily be lowered by simultaneously lengthening the heating time is clearly shown in fig. 8, where only 22 MW were applied for 30 seconds to otherwise the same case (shot NETb). A reduction factor 0.5 would lead to a much larger P_α, as shown in fig. 9 (44 MW for 15 sec were applied in this case, shot NETc).

Fig. 10 shows that a worse confinement could be cured by just increasing the average density: it refers to shot NETd, where the reduction factor was 0.7 (i.e. the enhanced confinement factor with respect to the L-mode was equal to 1.43), the average electron density was $1.17 \times 10^{20}\ \mathrm{m}^{-3}$ and 44 MW were applied for 30

seconds. Fig. 11 shows the possibility to operate for a substantial time interval (of the order of many energy confinement times) in a sub-ignited regime in which the α-power, in spite of being by far the dominating heating mechanism, is not very high, so that the heating loads are reduced and burn control is not required. This is obtained (shot NETe) by shutting off the additional heating just before the ignition point is reached. Note that shot NETe (fig. 11) differs from shot NETd (fig. 10) only in the heating time (25 seconds instead of 30 seconds). Already a heating time of 26 seconds would be enough to ignite, but 25 seconds are just not enough, and, after the shutting off of the additional power, the discharge dies slowly away, allowing the study of a 20-seconds long Ohmic phase with $P_\alpha = 80 \sim 100\,\mathrm{MW}$ and $P_\alpha/P_{Ohm} > 10$.

Of course, in all these simulations the temperature profile was Gaussian, because this is imposed by the transport model. The only way to get a broader temperature profile is to increase substantially the edge temperature (partly to simulate the temperature pedestal of the H-mode, partly just to get a broader temperature profile). In this case, no reduction factor is to be used for the heat conductivities, the improved confinement (with respect to the L-mode) being automatically obtained as a consequence of the high edge temperature. In fig. 12 a case is shown (shot NETf) where the temperature at the edge was set equal to 5 keV (resulting, at the end of the run, in a peaking factor for the temperature of the order of 2), the reduction factor was equal to 1, and 44 MW were applied for 15 seconds. For the rest shot NETf was identical to shot NETa.

Figure 13 shows the time behaviour of the powers for shot NT0b, which differs from shot NETa for the density profile (parabolic instead of square-root-of-parabolic), the reduction factor (0.7 instead of 0.6) and the heating time (28 seconds instead of 20). By comparing fig. 7 with fig. 13, we see that a worse confinement could also be cured by providing a less flat density profile.

Sawteeth will degrade the performance, but not dramatically. Fig. 14 (shot NETg) shows that, with a reduction factor 0.5 (i.e. an enhanced confinement factor with respect to the L-mode equal to 2) and the reference density ($0.9 \times 10^{20}\,\mathrm{m}^{-3}$), the desired performance is also obtained in the presence of Bohm diffusion (with coefficient 1) inside the magnetic surface $q = 1$ (which flattens the temperature profiles up to half radius). With a less pessimistic modelling of sawteeth (Bohm diffusion inside the magnetic surface $q = 0.9$, resulting in a temperature profile flat up to 2/5 of the radius) ignition is marginally obtained with a reduction factor 0.6. This is shown in fig. 15 (shot NETh). Finally, a simple sawtooth model was also used. In this model, ref. /13/, the sawtooth crash is modelled by a sudden flattening of the density and temperature (and safety factor) profiles inside the mixing region. The flattening (which conserves energy) takes place every time the value of the safety factor on axis reaches a given value $q_{crit} < 1$. This determines the sawtooth period. In these runs the density profile was allowed to evolve in time, with the same particle transport model used for IGNITOR, with a "weak" inward pinch as in the low and high field IGNITOR and in the NET reference runs. In shot NETi (fig. 16) this model was applied to the same parameters of shot NETa (apart from the heating time, 1 second longer), with $q_{crit} = 0.98$, which leads to a sawtooth period of 350 ms in the final phase of the discharge. In the same phase, the slowing down time for α-particles in the central part of the plasma is 600 ms: this explains the absence of fluctuations in $P_\alpha(t)$ in the figure. In spite of the presence of the sawteeth, this shot exhibits a performance very similar to that of shot NETa. This is probably due to the higher central density obtained as a combined effect of particle diffusion, particle pinch and flattening of the density at the sawtooth crash (compare fig. 16(c) with fig. 7(f)). In fig. 16(b) the ion temperature profiles just after a sawtooth crash (which happened at $t = 32.513$) and just before the following sawtooth crash (which happened at $t = 32.894$) are

shown. The electron temperature profiles have a similar behaviour. On the other hand, the electron and ion density profiles do not show appreciable variations during a sawtooth period. The shape they have at the end of the discharge (at $t = 35\,\mathrm{sec}$) is shown in fig. 16(c).

5.2 Conclusions

In conclusion, the Tang and Redi transport model predicts for NET II - 25 MA operating at the reference density and in the H-mode that NET ignites and has a good ignition margin. This can be quantified by the value of the enhancement factor of H-mode confinement (with respect to L-mode confinement), which is required to achieve ignition. This value is 1.67 for the nominal density and can be lower than 1.5 for a slightly larger (by 30%) average density or a more peaked (parabolic instead of square-root-of-parabolic) density profile. Sawteeth have been shown to have a relatively small effect, provided they do not lead to a large loss of the high-energy component of the α-particle population.

6. Overall Conclusions

An extensive numerical predictive study of IGNITOR discharges, a number of comparative runs for a NET-like plasma, and some runs for the NET II - 25 MA operating mode of NET have been performed using the Tang and Redi transport model and the $1\frac{1}{2}$-D transport code JETTO. The aim of this work was to assess the IGNITOR performance and the effect of size on it, and to compare IGNITOR with NET.

Firstly, it must be stressed that all the conclusions which are drawn here on the performance of IGNITOR and on the comparison IGNITOR-NET should be qualified as based on adopting the Tang and Redi transport model. Due to the still existing uncertainty regarding the physical mechanisms responsible for transport

in tokamaks and, as a consequence, regarding the tokamak transport coefficients, adopting the Tang and Redi model is an important assumption.

Actually, a comparison of the predictions of this model with a number of shots from different machines has shown that it tends to be optimistic for low-power discharges, the discrepancy decreasing as the power increases. This behaviour is due to the strongly unfavourable power dependence foreseen by the model, stronger than in most of the existing global scalings. Another feature of the Tang and Redi model which should be recalled here is its favourable scaling with density, and in particular with density peaking. All these dependencies favour small, high-density machines like IGNITOR with respect to larger, lower-field machines like NET. On the other hand, the Tang and Redi model, always in comparison with the existing scaling laws, has a relatively stronger (favorable) dependence on size and a relatively weaker (favourable) dependence on the magnetic field intensity. This favors large, low-field machines with respect to smaller, higher field machines, more than other scalings. Therefore, the model does not have a clear bias towards one of the two types of devices. A peculiar aspect of the Tang and Redi model is the fact that it can exhibit bifurcation, as discussed in detail in section 3.2 in connection with shots LFd to LFg.

From the IGNITOR simulations, the conclusion has been drawn that many conditions have to be simultaneously fulfilled to obtain IGNITOR discharges in which, within the flat-top time, α-particle heating becomes the dominant heating mechanism. From the simulations of the NET-like plasma, it appears clearly that in this large-size plasma, ignition is more easily reached. Finally, from the simulations of the NET II - 25 MA operating scenario of NET, it was confirmed that ignition can be obtained in NET, in the H-mode, under a variety of conditions.

Acknowledgements

Multiple discussions with Drs. F. Engelmann and F. Troyon have greatly influenced this study. The assistance of Dr. A. Taroni in setting up the code JETTO for our use has been invaluable. Discussions with Drs. G. Cenacchi and F. Hofmann have been sincerely appreciated. Computer assistance has been provided by B. Esser.

References

/1/ B. Coppi, Vuoto XVII, 153 (1988).

/2/ G. Cenacchi and A. Taroni, JET Internal report JET-IR(88)03 (1988).

/3/ W. M. Tang, Nucl. Fusion 26, 1605 (1986).

/4/ M. H. Redi, W. M. Tang, P. C. Efthimion, D. R. Mikkelsen and G. L. Schmidt, Nucl. Fusion 27, 2001 (1987).

/5/ NET TEAM, Plasma Physics and Controlled Nuclear Fusion Research 1988, Twelfth Conference Proceedings, Nice, 12-19 October 1988, 3, 287 (1989).

/6/ R. W. Ross, P. H. Diamond, J. F. Drake, F. L. Hinton, F. W. Perkins, W. M. Tang, R. E. Waltz and S. J. Zweben, University of Texas Fusion Research Center Report FRCR #295 (1987).

/7/ A. Airoldi and G. Cenacchi, Istituto di Fisica del Plasma, CNR, Milano, Internal Report FP 89/9 (1989).

/8/ C. S. Chang and F. L. Hinton, Phys. Fluids 29, 3314 (1986).

/9/ B. Coppi and N. Sharky, Nucl. Fusion 21, 1363 (1981).

/10/ Yushmanov P., Takizuka T., Riedel K., Kardaun O., Cordey J., Kaye S. and Post D., ITER Internal Report ITER-IL-Ph-4-9-7 (1989), submitted to Nuclear Fusion.

/11/ Corrigan C., Düchs D. F., Nocentini A., Sack Ch., Springmann E., Stringer T. E., Taroni A. and Tibone F., Proc. 17th EPS Conference on Controlled Fusion and Plasma Heating, 25-29 June 1990, Amsterdam (NL), 801 (1990).

/12/ Gruber O., Wunderlich R., Lackner K. and Schneider W., IPP Internal Report IPP 5/29 (1989).

/13/ Kadomtsev B. B., Soviet J. Plasma Phys. Vol.1, p.389 (1975), and A. Taroni and F. Tibone, JET report JET-DN-T(85) (1985).

Figure Captions

1.ASDEX-shot. In (a) the measured and calculated profiles of electron and ion temperatures are given. In (b) the electron heat conductivity and the ion heat conductivity (full line) and, for comparison, the neoclassical ion heat conductivity (dashed line) before having taken into account the volume correction due to the shape of the equilibrium magnetic surfaces, in (c) the time dependence of the loop voltage and the energy confinement time is given.

2.LF0. The "low field reference run". In (a) the time dependence of the powers is given (A = Ohmic power, B = alpha power, C = bremsstrahlung, E = impurity radiation); in (b) and (c) the time dependence of the energy confinement time and the loop voltage, respectively, is given; in (d) and (e) the initial and final electron density and central electron temperature profiles are plotted (t=0.0 s is dashed, t=7.0 s is solid); in (f), (g), (h) and (i) the profiles (at t=3.2s) of the following quantities are given: electron heat conductivity (f); Ohmic power density (g); current density (h); safety factor (i), observe: $q_0 = 0.7$.

3.LGg. In (a) the time dependence of the powers is given (A = Ohmic power, B = alpha power, C = bremsstrahlung, E = impurity radiation); in (b) and (c) the time dependence of the energy confinement time and loop voltage, respectively, is given; in (d) and (e) the initial and final electron density and central electron temperature profiles are plotted (t=0.0 s is dashed, t=7.0 s is solid); in (f), (g), (h) and (i) the profiles (at t=4.0s) of the following quantities are given: electron heat conductivity (f); Ohmic power density (g); current density (h); safety factor (i), observe: $q_0 = 0.7$.

4.HF0. The "high field reference run". In (a) the time dependence of the powers

is given (A = Ohmic power, B = alpha power, C = bremsstrahlung, E = impurity radiation); in (b) and (c) the time dependence of the energy confinement time and loop voltage, respectively, is given; in (d) and (e) the initial and final electron density and central electron temperature profiles are plotted (t=0.0 s is dashed, t=7.0 s is solid); in (f), (g), (h) and (i) the profiles (at t=4.0s) of the following quantities are given: electron heat conductivity (f); Ohmic power density (g); current density (h); safety factor (i), observe: $q_0 = 0.7$.

5.LFe. In (a), the time dependence of the powers is given (A = Ohmic power, B = alpha power, C = bremsstrahlung, E = impurity radiation), and in (b), (c) and (d) is given the time dependence of the energy confinement time (b), the average (c) and central (d) electron (full line) and ion (dashed line) temperatures.

6.NET. The NET reference run with 13 sec of additional heating (NT0a). In (a) the time dependence of the powers is given (A = Ohmic power, B = alpha power, C = bremsstrahlung, D = additional power, E = impurity radiation); in (b) and (c) the time dependence of the energy confinement time and loop voltage , respectively, is given; in (d) the initial and final electron density profiles are plotted (t=0 s is dashed, t=20 s is solid); in (e), (f), (g) and (h) the final profiles (at t=20s) of the following quantities are given: electron heat conductivity (e); electron (full line) and ion (dashed line) temperatures (f); current density (g); safety factor (h), observe: $q_0 = 0.7$.

7.NETa. In (a) the time dependence of the powers is given (A = Ohmic power, B = alpha power, C = bremsstrahlung, D = additional power, E = impurity radiation); in (b) and (c) the time dependence of the energy confinement

time and the loop voltage, respectively, is given; in (d) the power loss (P_χ) due to the heat conductivities of electrons (full line) and ions (dashed line) are given; in (e) the average temperatures of electrons (full line) and ions (dashed line) are given; in (f), (g), (h), (i), (j), (k) and (l) the profiles (at t=35s) of the following quantities are given: electron (full line) and main ion (dashed line) densities (f) and temperatures (g), electron heat conductivity (h); Ohmic power density (i); current density (j); safety factor (k), observe: $q_0 = 0.7$; ion heat conductivity (full line) and its neoclassical part (dashed line) (l).

8.NETb. The time dependence of the powers is given (A = Ohmic power, B = alpha power, C = bremsstrahlung, D = additional power, E = impurity radiation).

9.NETc. The time dependence of the powers is given (A = Ohmic power, B = alpha power, C = bremsstrahlung, D = additional power, E = impurity radiation).

10.NETd. The time dependence of the powers is given (A = Ohmic power, B = alpha power, C = bremsstrahlung, D = additional power, E = impurity radiation).

11.NETe. The time dependence of the powers is given (A = Ohmic power, B = alpha power, C = bremsstrahlung, D = additional power, E = impurity radiation).

12.NETf. The time dependence of the powers is given (A = Ohmic power, B = alpha power, C = bremsstrahlung, D = additional power, E = impurity radiation).

13.NTOb. The time dependence of the powers is given (A = Ohmic power, B =

alpha power, C = bremsstrahlung, D = additional power, E = impurity radiation).

14.NETg. In (a) the time dependence of the powers is given (A = Ohmic power, B = alpha power, C = bremsstrahlung, D = additional power, E = impurity radiation); in (b) the electron (full line) and ion (dashed line) temperature profiles at $t = 30$ sec are given.

15.NETh. In (a), the time dependence of the powers is given (A = Ohmic power, B = alpha power, C = bremsstrahlung, D = additional power, E = impurity radiation); in (b) the electron (full line) and ion (dashed line) temperature profiles at $t = 50$ sec are given.

16.NETi. In (a) the time dependence of the powers is given (A = Ohmic power, B = alpha power, C = bremsstrahlung, D = additional power, E = impurity radiation); in (b) the ion temperature profile at $t = 32.53$ (just after a sawtooth crash, full line) and at $t = 32.88$ (just before the following sawtooth crash, dashed line) are shown; in (c) the electron (full line) and main ion (dashed line) density profiles at the end of the discharge ($t = 35$ sec) are shown.

TABLE I

Run	t_1	t_2	t_4	t_{10}	$\Re(7)$	P'_α	P''_α	Notes
LF0	1.9	3.4			3.5	+	−	$\bar{Z} = 1.2$, $\bar{n}_e = 5.8 \times 10^{20} m^{-3}$
LF0r	1.7	2.3	3.2	5.7	11.6	+	−	eq. recalculated at .5, 1., 2., 4.
Sensitivity to Initial temperature:								
LF1	2.3	Halved initial temperatures; shot ended at $t = 2.3$ sec						
Sensitivity to sawteeth :								
LF2a					0.43	0	0	0.1 Bohm for $q < 0.8$
LF2b					0.42	0	0	0.1 Bohm for $q < 0.7$; $q_0 = 0$; eq. recalc.
LF2c					0.17	0	0	reconnection for $q < 0.1$ when $q(0) < 0.8$
Sensitivity to heat diffusion intensity :								
LF3					0.04	0	0	χ_e increased by 25%
Sensitivity to Z_{eff} :								
LF4	3.0				1.5	+	−	$\bar{Z} = 1.33$ (double impurity content)
LF4a					0.9	0	−	$\bar{Z} = 1.46$ (triple impurity content)
Sensitivity to the ion central density :								
LF5	1.4				1.6	0	0	20% smaller than in LF0
Sensitivity to the initial profile :								
LF5a					0.24	0	0	quadratic profile
Sensitivity to deuterium-tritium ratio :								
LF6	3.3				1.1	0	0	70% deuterium and 30% tritium
Sensitivity to the value of the current :								$I_p(MA)$ (= 10.0 in LF0)
LF7	3.9				1.1	0	0	9.0
LF7a	3.5				0.97	0	0	9.0; moreover: 20% lower density
Sensitivity to edge temperature :								$T_{edge}(\infty)$ (= 0.6 keV in LF0)
LF8a	2.1	4.8			2.1	0	0	0.4
LF8b					0.05	0	0	0.3
LF8c	2.1	2.7	3.4	4.1	$\Re(6) = 113.$			$T_{edge}(t > 2) = 1.2$ keV
Sensitivity to particle pinch :								α_{inw} (= 3 in LF0)
LF9	1.9	4.3			2.0	0	0	2.0

TABLE II

Run	t_1	t_2	t_4	t_{10}	$\Re(7)$	P'_α	P''_α	Notes
LFa					0.05	0	0	$\alpha_{inw} = 2.0$
LFb	1.8	3.1			2.6	0	0	$\alpha_{inw} = 3.0$
LFc	1.7	2.2	2.8	3.5	97.	+	−	$\alpha_{inw} = 10.$
								$n_e(0)/\bar{n}_e$, see text
LFd					0.13	0	0	2.3 at $7s$
LFe	5.6	6.9			2.1	+	0	2.2 at $4.3s$
LFf	3.2	4.3	5.7		9.9	+	+	2.1 at $1.9s$
LFg	2.6	3.6	4.6	5.7	44.	+	+	2.0 at $1.2s$

TABLE III

Run	t_1	t_2	t_4	t_{10}	$\Re(7)$	P'_α	P''_α	Notes
LFg	2.6	3.6	4.6	5.7	44.	+	+	$\bar{Z} = 1.2$, $\bar{n}_e = 6.2 \times 10^{20} m^{-3}$
Sensitivity to χ_i^{anom} :								(neoclassical in LFg)
LFg1a	3.7	4.5	5.5		3.6	+	0	$\eta_c = 0.6$
LFg1b					0.4	0	0	$\eta_c = 0.4$
Sensitivity to edge temperature :								$T_{edge}(\infty)(= 0.6\,\mathrm{keV}$ in LFg)
LFg2a	6.7				1.2	+	+	0.3
LFg2b					.04	0	0	0.2
Sensitivity to Bohm diffusion :								no Bohm diffusion in LFg
LFg3					0.5	0	0	0.1 Bohm for $q < 0.8$
Sensitivity to heat diffusion intensity :								
LFg4					0.6	0	0	$\chi_{e,i}$ increased by 25%
Sensitivity to Z_{eff} :								$\bar{Z}$, $\bar{n}_{e,14}$, $\bar{n}_{C,12}$, $\bar{n}_{O,11}$
LFg5a	3.3	6.2			2.3	+	0	1.4, 5.7, 6.2, 6.2
LFg5b	3.5	6.2			2.4	+	+	1.4, 6.1, 6.3, 6.3
LFg5c					0.7	+	−	1.6, 6.3, 9.4, 9.4
LFg5d					0.8	+	−	1.6, 6.2, 9.4, 9.4
LFg5e					0.8	+	−	1.6, 6.1, 9.4, 9.4
Sensitivity to q_{min} :								
LFg6a	2.8	3.7	4.7	5.7	42.	+	+	$q_{min} > 0.8$
LFg6b	3.1	4.0	4.9	5.9	36.	+	+	$q_{min} > 0.9$
LFg6c	3.9	4.7	5.5	stop at 6.6 sec				$q_{min} > 1.0$; χ_i^{anom} for $t \geq 5.7$

TABLE IV

Run	t_1	t_2	t_4	t_{10}	$\Re(7)$	P'_α	P''_α	Notes
HF0	0.9	1.3	1.8	3.7	11.5	0	0	$\bar{Z} = 1.25$, $\bar{n}_e = 4.6 \times 10^{20}$
HF0r	0.9	1.4	1.9		$\Re\,(4) = 5.7$			eq. recalculated at .5, 1., 2., 4. sec
Sensitivity to sawteeth :								
HF1	0.9	1.4			1.6	0	+	0.1 Bohm for $q < 0.8$
Sensitivity to heat diffusion intensity :								
HF2	1.7				1.0	0	0	χ_e increased by 25%
Sensitivity to Z_{eff} :								
HF3	1.1	1.9	3.0		7.3	0	0	$Z_{eff} = 1.43$ (double impurity content)
Sensitivity to deuterium-tritium ratio :								
HF4	1.1	2.2			3.5	0	0	70% deuterium and 30% tritium
Sensitivity to particle pinch :								
HF5	0.9	1.5	2.5		3.6	−	+	$\alpha_{inw} = 2.0$
Sensitivity to smoothing of η_i-threshold :								
HF6a1	0.9	1.2	1.7	3.3	11.3	0	−	$z = 20$ eq. recalculated
HF6a2	0.9	1.3	1.7		8.1	0	0	$z = 5$ eq. recalculated
HF6b1	0.9	1.3	1.9		9.6	0	0	$z = 4$
HF6b2	0.9	1.4	2.1		7.2	0	0	$z = 2$

TABLE V

Run	t_1	t_2	t_4	t_{10}	$\Re(10)$	P'_α	P''_α	Notes
NT0	3.5	4.3	5.2	6.5	72.	+	+	$\bar{Z} = 1.9$, $\bar{n}_e = 0.9 \times 10^{20}$, parabolic
NT0a	$13s$ heating pulse; $\Re(t > 15) = 307.$							$P_\alpha = 486\,\mathrm{MW}$ for $t > 15s$
NT0b	$28s$ heating pulse $(44MW)$; χ_i^{anom}; $\chi \times 7/8$							$P_\alpha > 225\,\mathrm{MW}$ for $t > 30s$
Sensitivity to the introduction of χ_i^{anom} :								(neoclassical for $t > 4\,\mathrm{sec}$ in NT0)
NT1a	3.5	4.5	5.7	7.7	22.	+	−	$P_\alpha(t = 20) = 225\,\mathrm{MW}$
NT1b	$13s$ heating pulse; $P_\alpha^{max} = 200\,\mathrm{MW}$							goes back to Ohmic
NT1c	$20s$ heating pulse; $P_\alpha^{max} = 260\,\mathrm{MW}$							goes back to Ohmic
NT1d	$30s$ heating pulse; $P_\alpha^{max} = 300\,\mathrm{MW}$							goes back to Ohmic
Sensitivity to edge temperature :								$T(a, t > 1)(= 0.6\,\mathrm{keV}$ in NT0)
NT2	4.5	5.3	6.2	7.5	43.	+	+	0.3,
Sensitivity to Bohm diffusion ($q_0 = 0$) :								no Bohm diffusion in NT0
NT3a	3.5	4.3	5.2	6.5	72.	+	+	$0.1 \times \chi^{Bohm}$ for $q < 0.7$
NT3b	3.5	4.3	5.2	6.5	71.	+	+	$0.1 \times \chi^{Bohm}$ for $q < 0.8$
NT3c	3.5	4.4	5.3	6.7	63.	+	+	$0.1 \times \chi^{Bohm}$ for $q < 0.9$
NT3d	3.5	4.5	5.4	6.9	53.	+	+	$0.1 \times \chi^{Bohm}$ for $q < 1.0$
NT3e	3.7	4.6	5.6	7.1	39.	+	+	$1.0 \times \chi^{Bohm}$ for $q < 1.0$
Sensitivity to heat diffusion intensity :								
NT4	6.4	8.1	9.5		5.2	+	+	$1.5 \times \chi_{e,i}$
Lower power input (62 MW) and Bohm diffusion for $q < 1$								
NT5a	$15s$ heating pulse; $R(t > 17) = 45.$							$P_\alpha = 170\,\mathrm{MW}$ for $t > 17s$
NT5b	$20s$ heating pulse; $R(t > 22) = 120.$							$P_\alpha = 250\,\mathrm{MW}$ for $t > 22s$

Figure 1 (a)

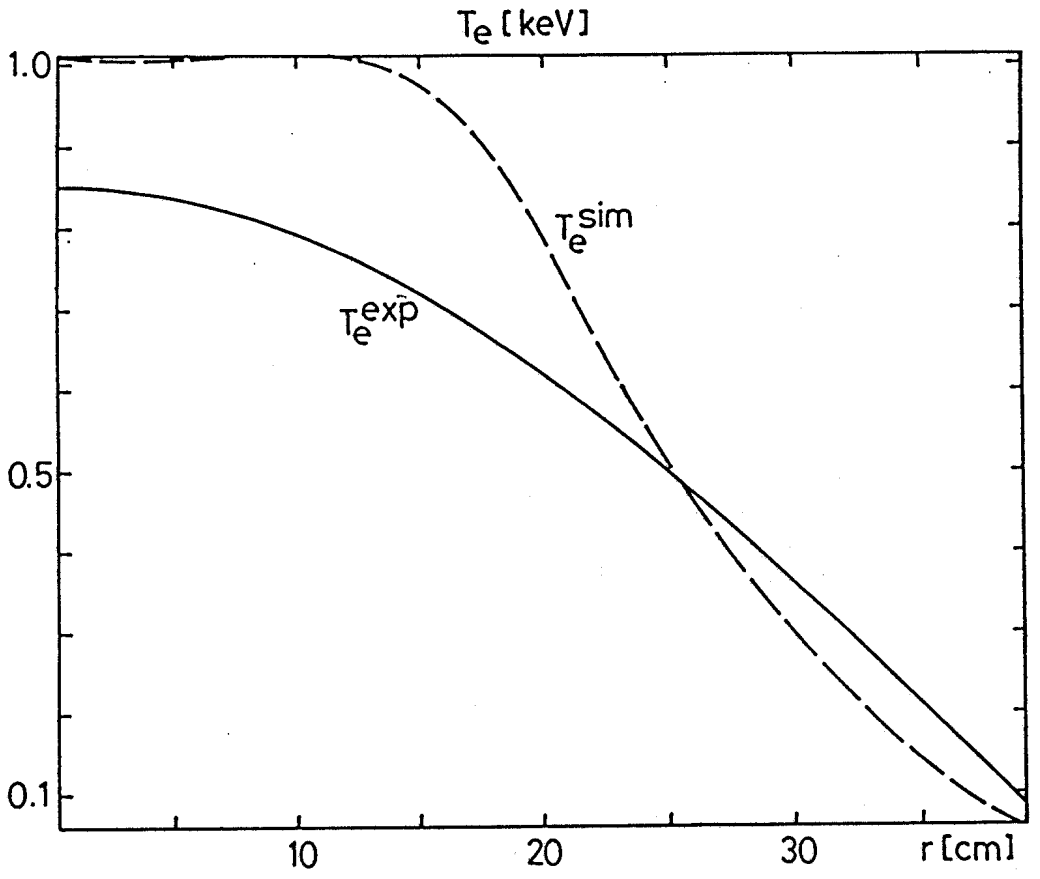
T_e [keV]
1.0
0.5
0.1
T_e^{sim}
T_e^{exp}
10
20
30
r [cm]

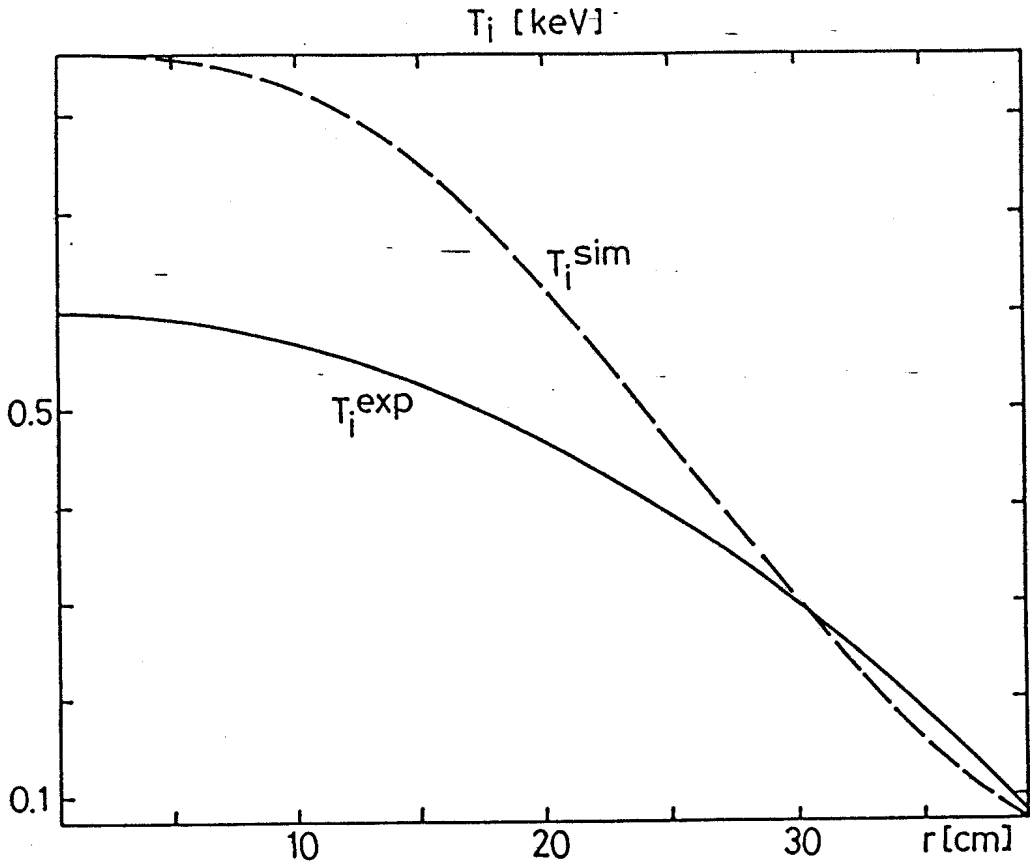
T_i [keV]
0.5
0.1
T_i^{sim}
T_i^{exp}
10
20
30
r [cm]

Figure 1

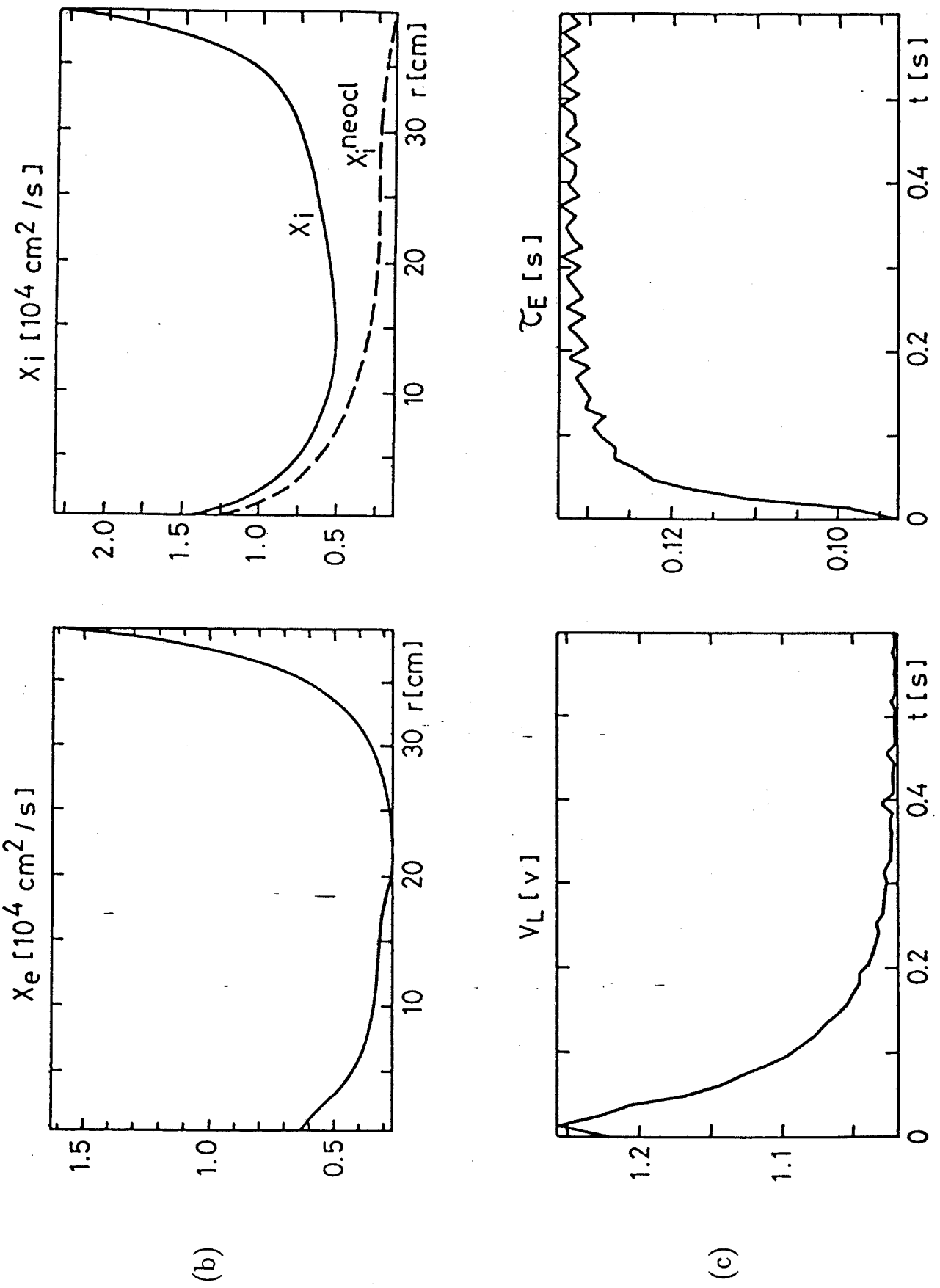
(b)
χ_i [10^4 cm^2/s]
χ_i
χ_i^{neocl}
r[cm]
χ_e [10^4 cm^2/s]
r[cm]
(c)
τ_E [s]
t [s]
V_L [v]
t [s]

Figure 2

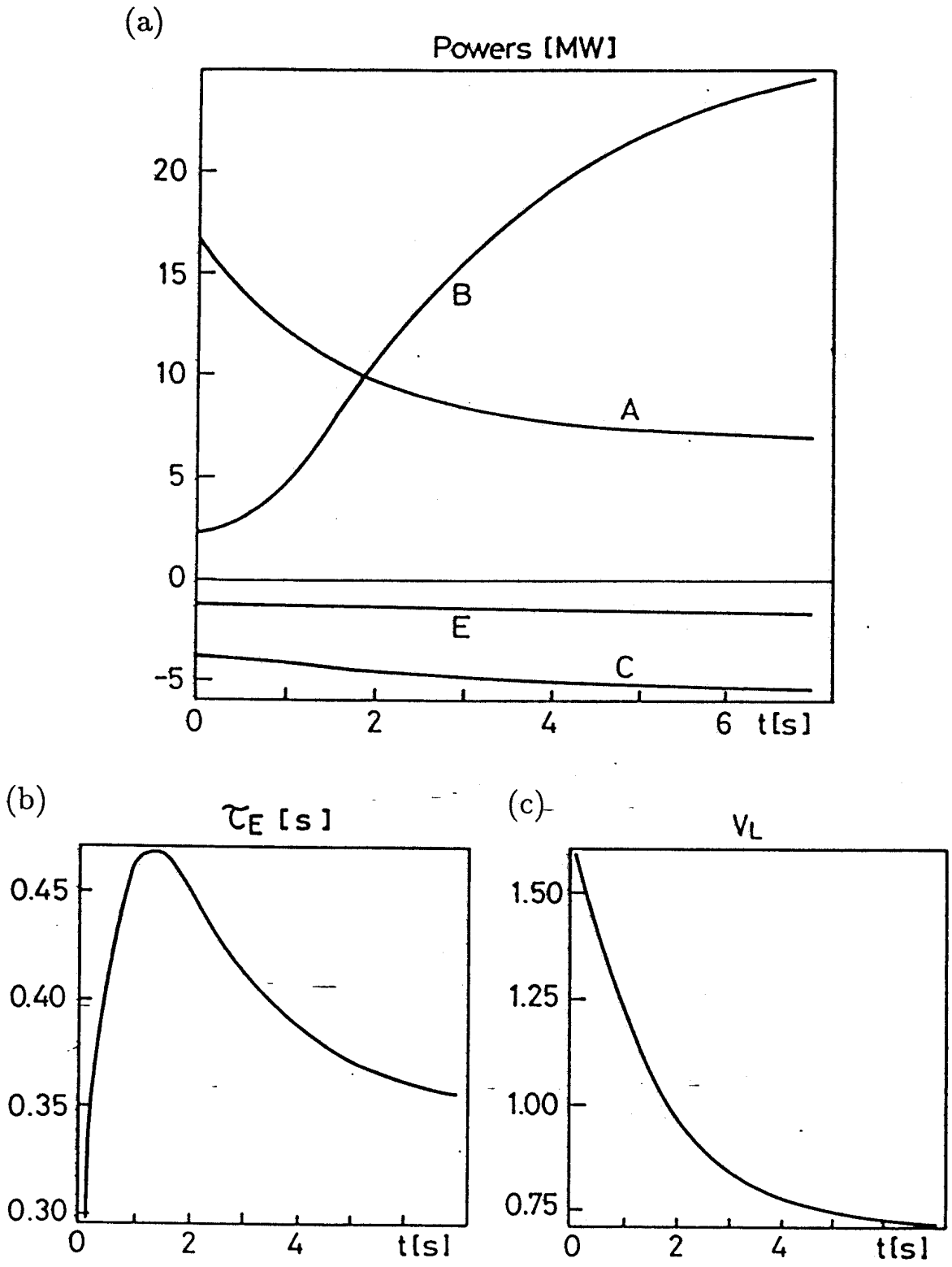
(a)
Powers [MW]
20
15
10
5
0
-5
B
A
E
C
0
2
4
6 t[s]
(b)
τ_E [s]
0.45
0.40
0.35
0.30
0
2
4
t[s]
(c)
V_L
1.50
1.25
1.00
0.75
0
2
4
t[s]

Figure 2

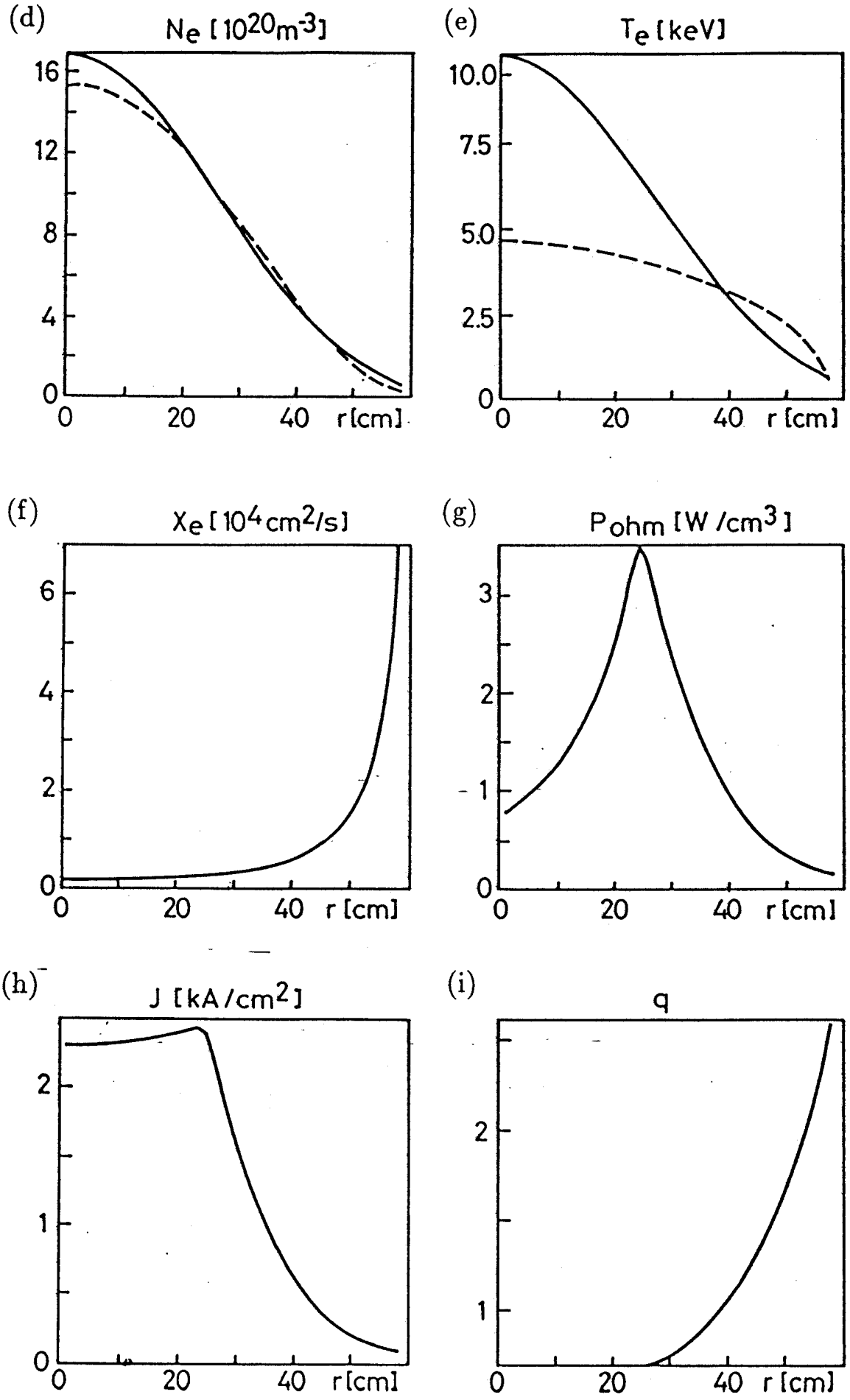
(d)
Ne [10^20 m^-3]
16
12
8
4
0
0
20
40
r [cm]
(e)
Te [keV]
10.0
7.5
5.0
2.5
0
0
20
40
r [cm]
(f)
Xe [10^4 cm^2/s]
6
4
2
0
0
20
40
r [cm]
(g)
Pohm [W/cm^3]
3
2
1
0
0
20
40
r [cm]
(h)
J [kA/cm^2]
2
1
0
0
20
40
r [cm]
(i)
q
2
1
0
20
40
r [cm]

Figure 3

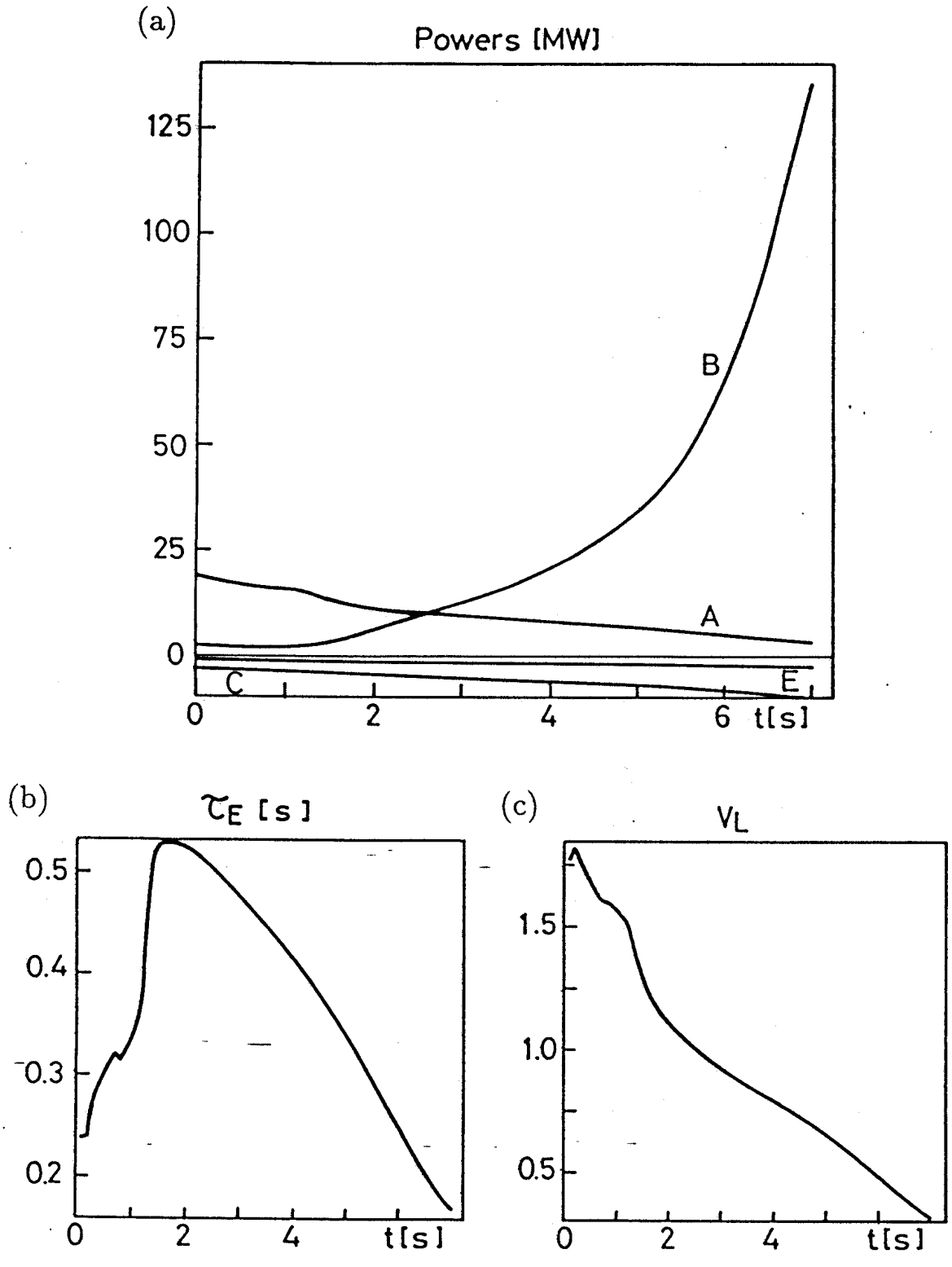
(a)
Powers [MW]
125
100
75
50
25
0
B
A
C
E
0
2
4
6 t[s]
(b)
τ_E [s]
0.5
0.4
0.3
0.2
0
2
4
t[s]
(c)
V_L
1.5
1.0
0.5
0
2
4
t[s]

Figure 3

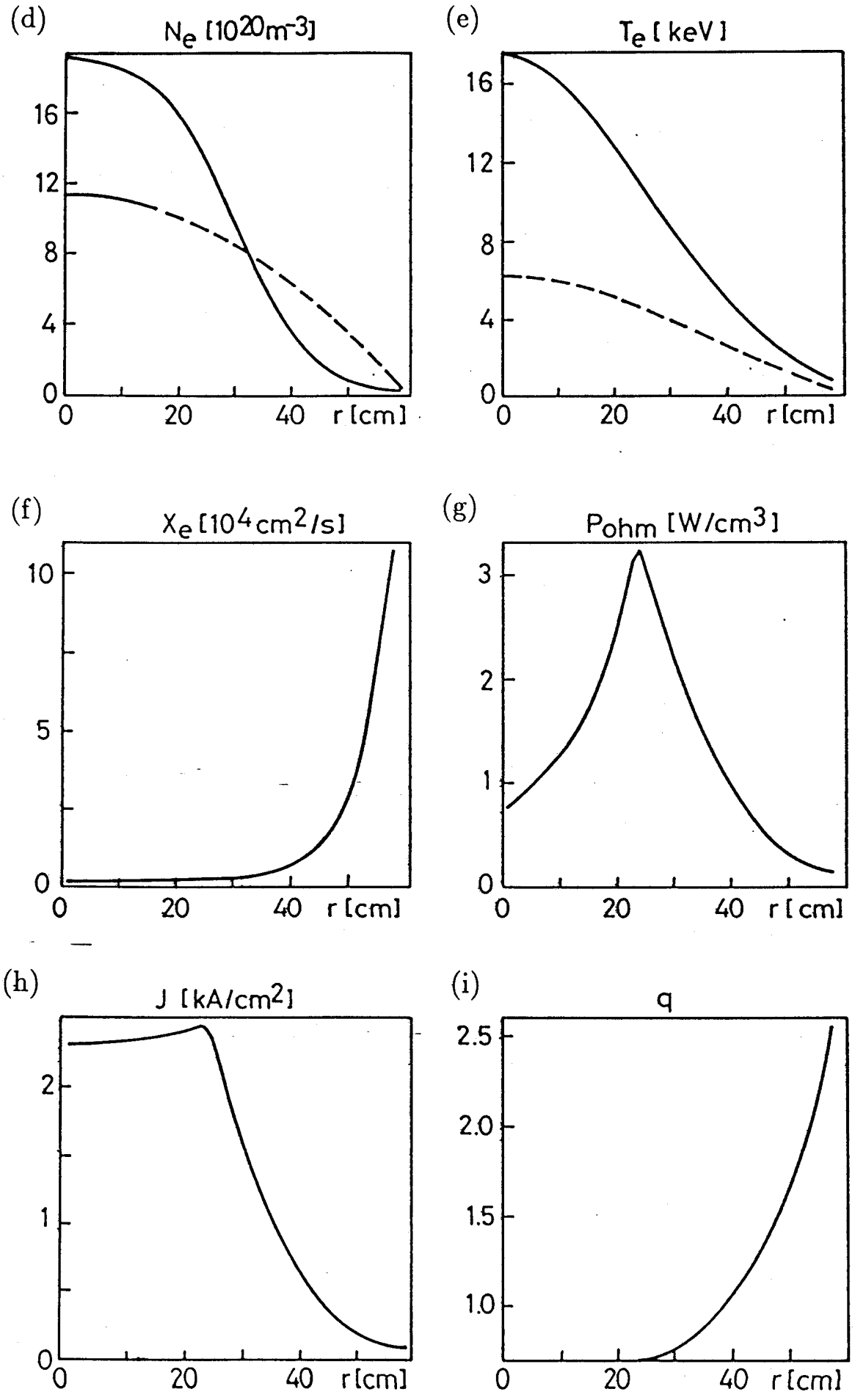
(d)
N_e [$10^{20}m^{-3}$]
16
12
8
4
0
0
20
40
r [cm]
(e)
T_e [keV]
16
12
8
4
0
0
20
40
r [cm]
(f)
X_e [$10^4 cm^2/s$]
10
5
0
0
20
40
r [cm]
(g)
P_{ohm} [W/cm^3]
3
2
1
0
0
20
40
r [cm]
(h)
J [kA/cm^2]
2
1
0
0
20
40
r [cm]
(i)
q
2.5
2.0
1.5
1.0
0
20
40
r [cm]

Figure 4

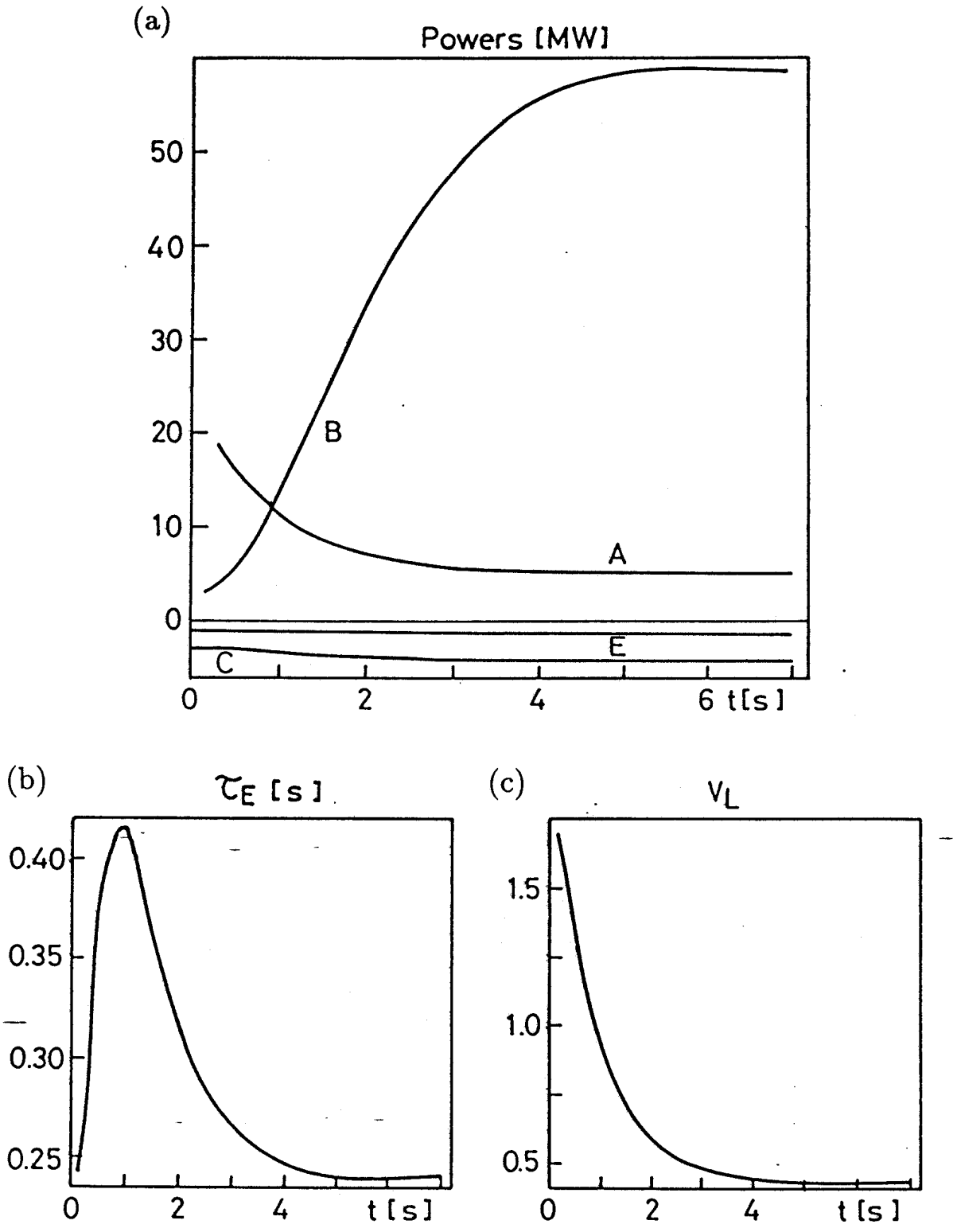
(a)
Powers [MW]
50
40
30
20
10
0
B
A
E
C
0
2
4
6 t[s]
(b)
τ_E [s]
0.40
0.35
0.30
0.25
0
2
4
t [s]
(c)
V_L
1.5
1.0
0.5
0
2
4
t [s]

Figure 4

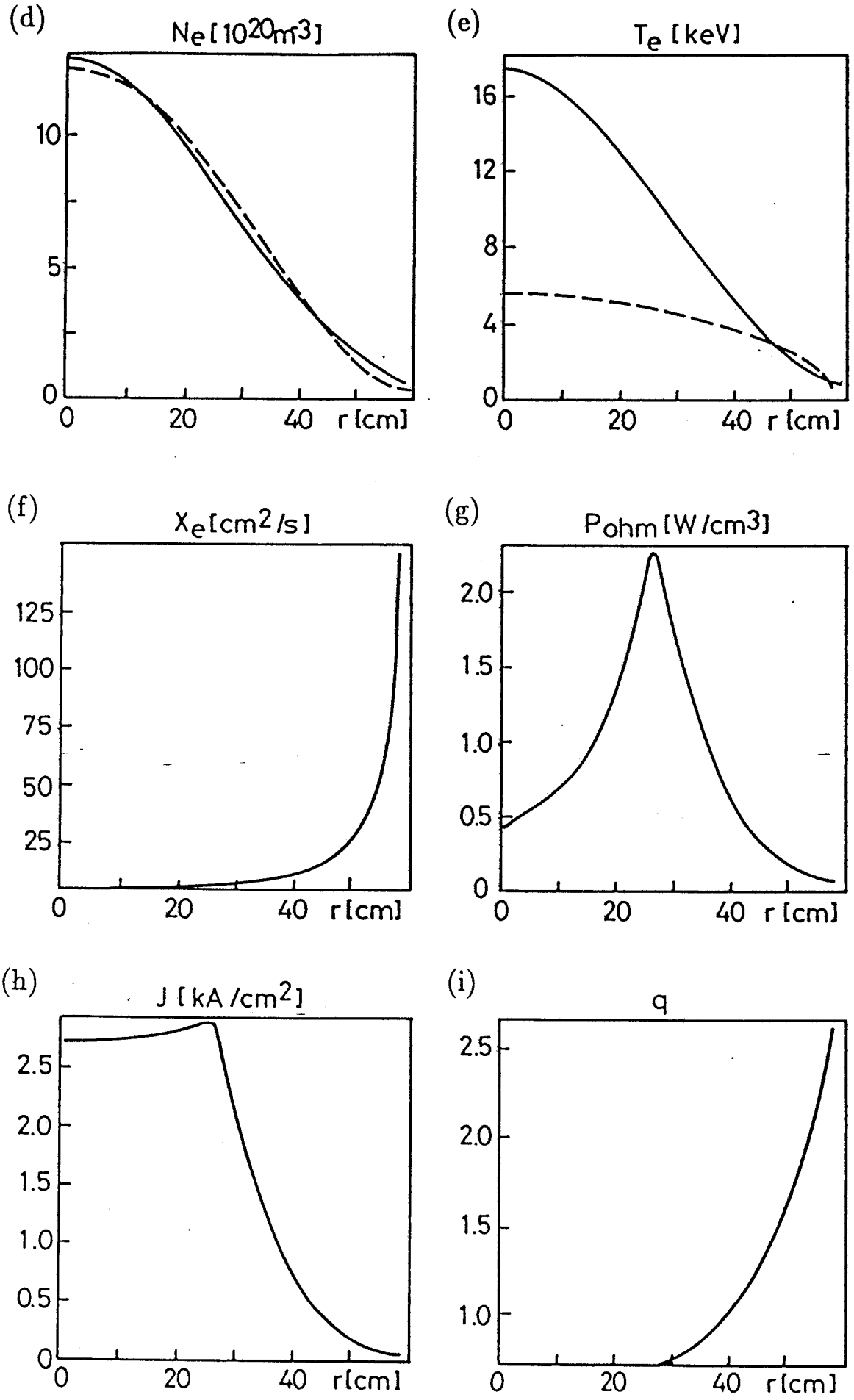
(d)
Ne[10^20m^3]
10
5
0
0
20
40
r[cm]
(e)
Te [keV]
16
12
8
4
0
0
20
40
r [cm]
(f)
Xe[cm^2/s]
125
100
75
50
25
0
20
40
r[cm]
(g)
Pohm [W/cm3]
2.0
1.5
1.0
0.5
0
0
20
40
r [cm]
(h)
J [kA/cm^2]
2.5
2.0
1.5
1.0
0.5
0
0
20
40
r[cm]
(i)
q
2.5
2.0
1.5
1.0
0
20
40
r[cm]

Figure 5

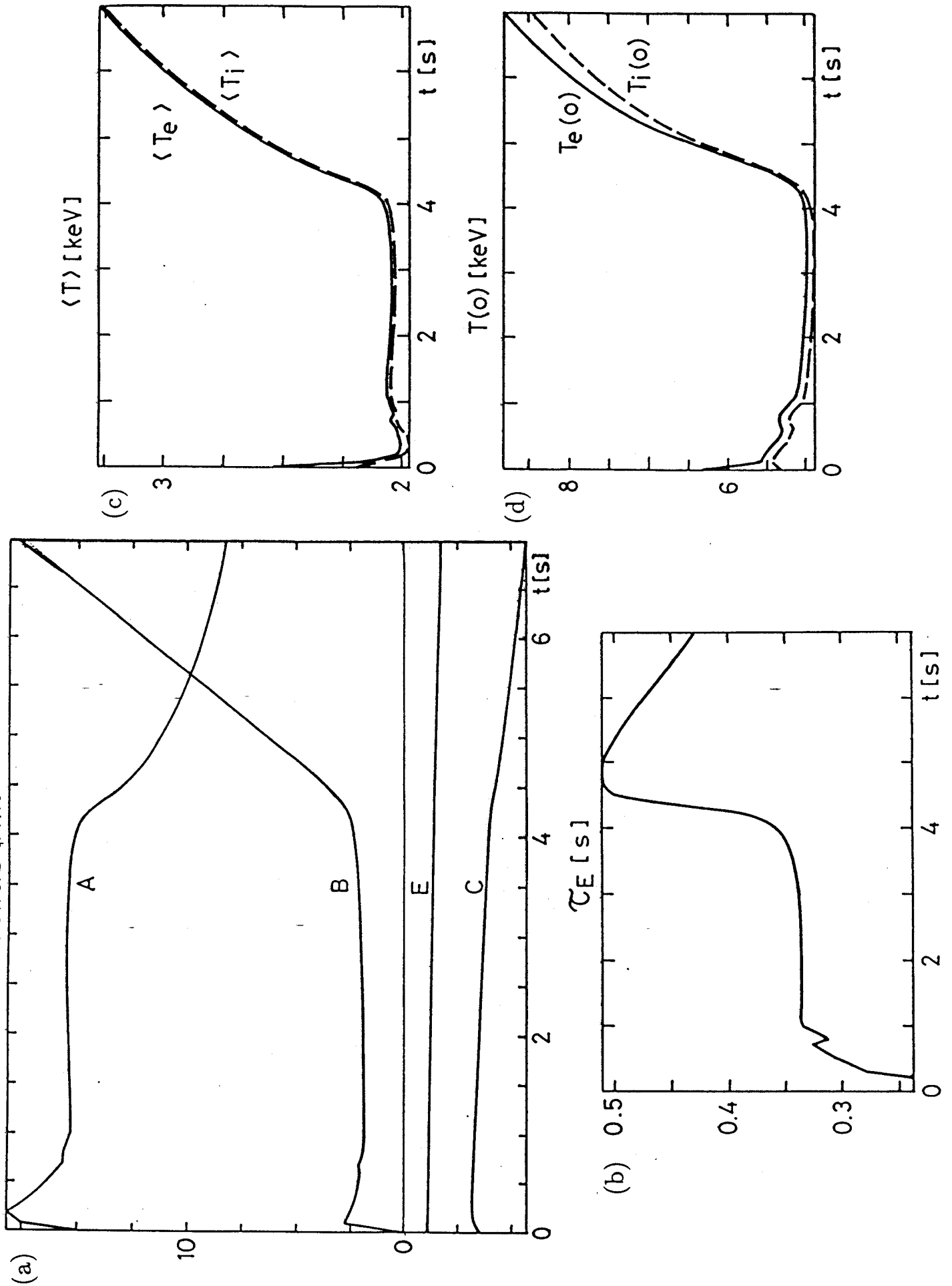

Figure 6

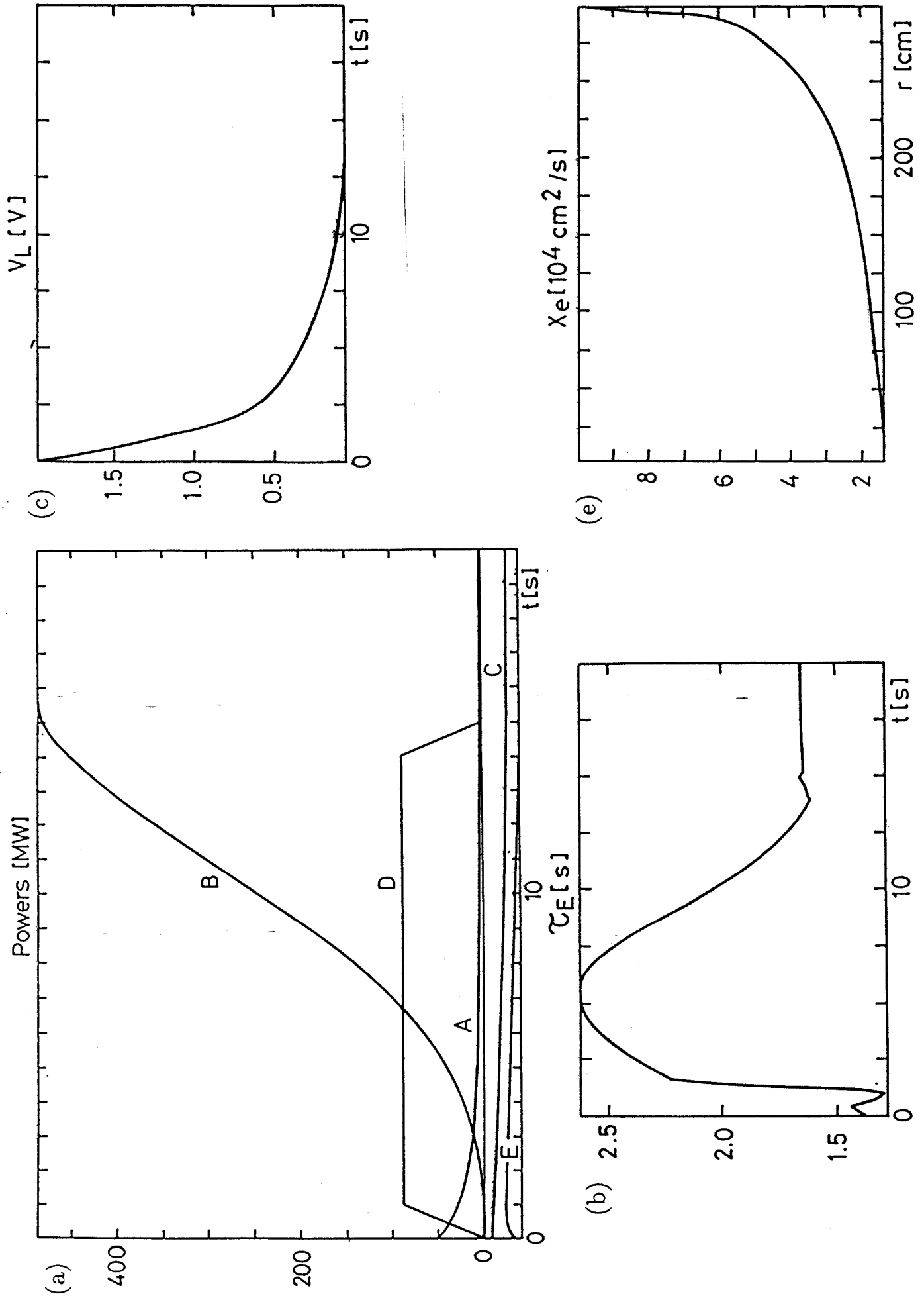
(a)
Powers [MW]
400
200
0
A
B
C
D
E
0
10
t [s]
(b)
τ_E [s]
2.5
2.0
1.5
0
10
t [s]
(c)
V_L [V]
1.5
1.0
0.5
0
10
t [s]
(e)
χ_e [10^4 cm^2/s]
8
6
4
2
100
200
r [cm]

Figure 6

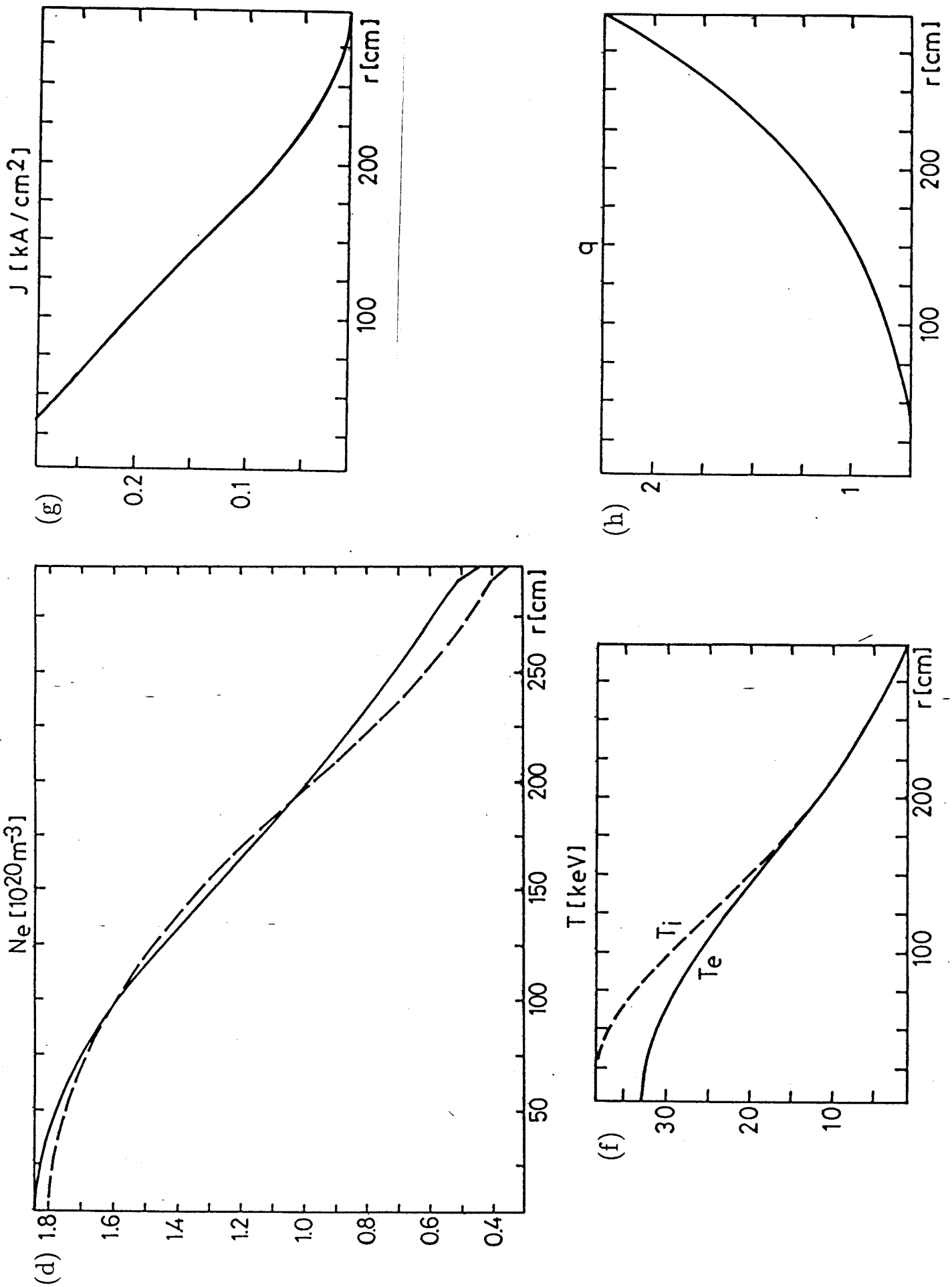
(g)
J [kA/cm2]
0.2
0.1
100
200
r [cm]
(h)
q
2
1
100
200
r [cm]
(d)
Ne [10^20 m^-3]
1.8
1.6
1.4
1.2
1.0
0.8
0.6
0.4
50
100
150
200
250
r [cm]
(f)
T [keV]
Ti
Te
30
20
10
100
200
r [cm]

Figure 7

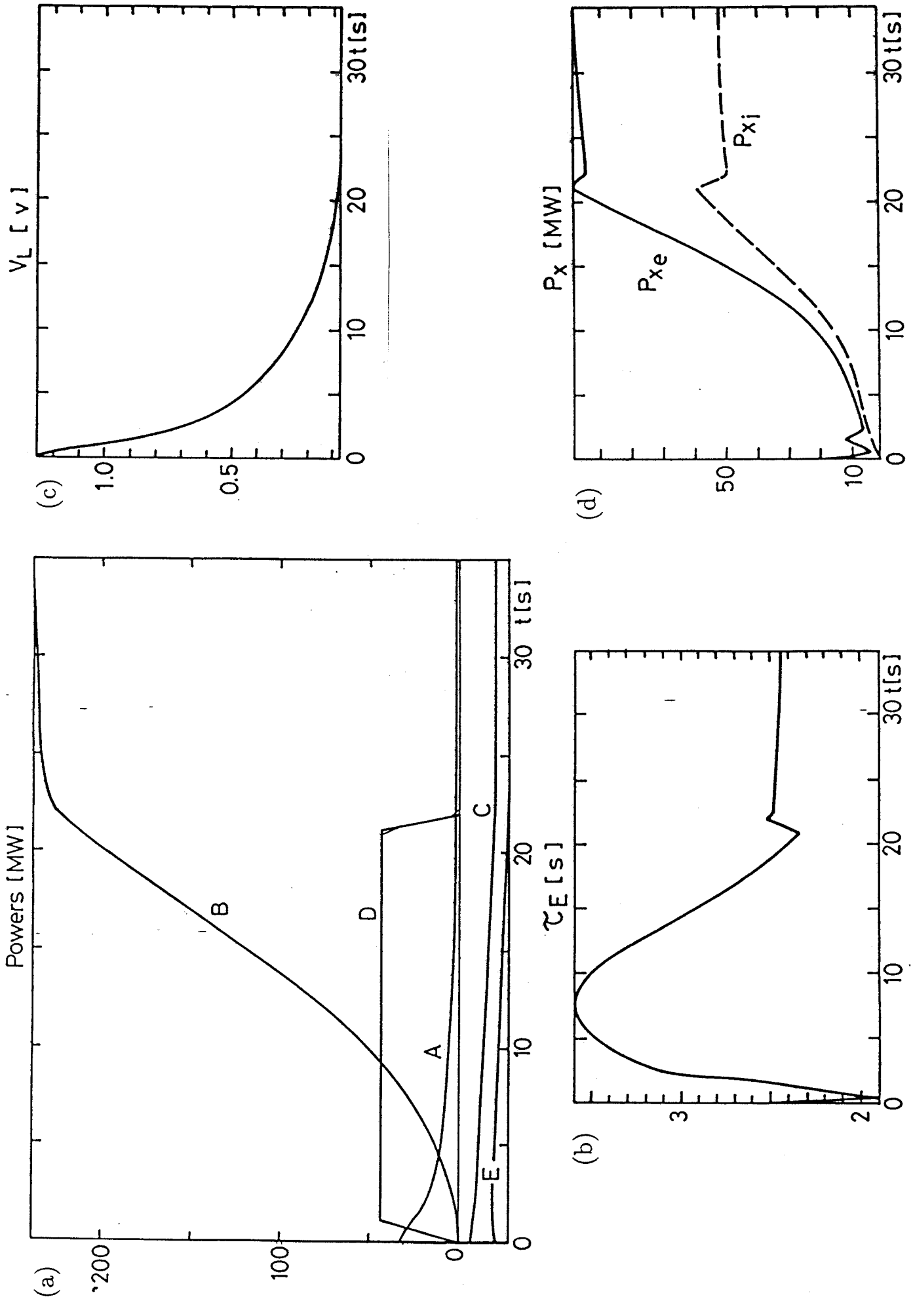
(a)
Powers [MW]
200
100
0
A
B
C
D
E
0
10
20
30 t[s]
(b)
τ_E [s]
3
2
0
10
20
30 t[s]
(c)
V_L [v]
1.0
0.5
0
10
20
30 t[s]
(d)
P_x [MW]
P_{xe}
P_{xi}
50
10
0
10
20
30 t[s]

Figure 7

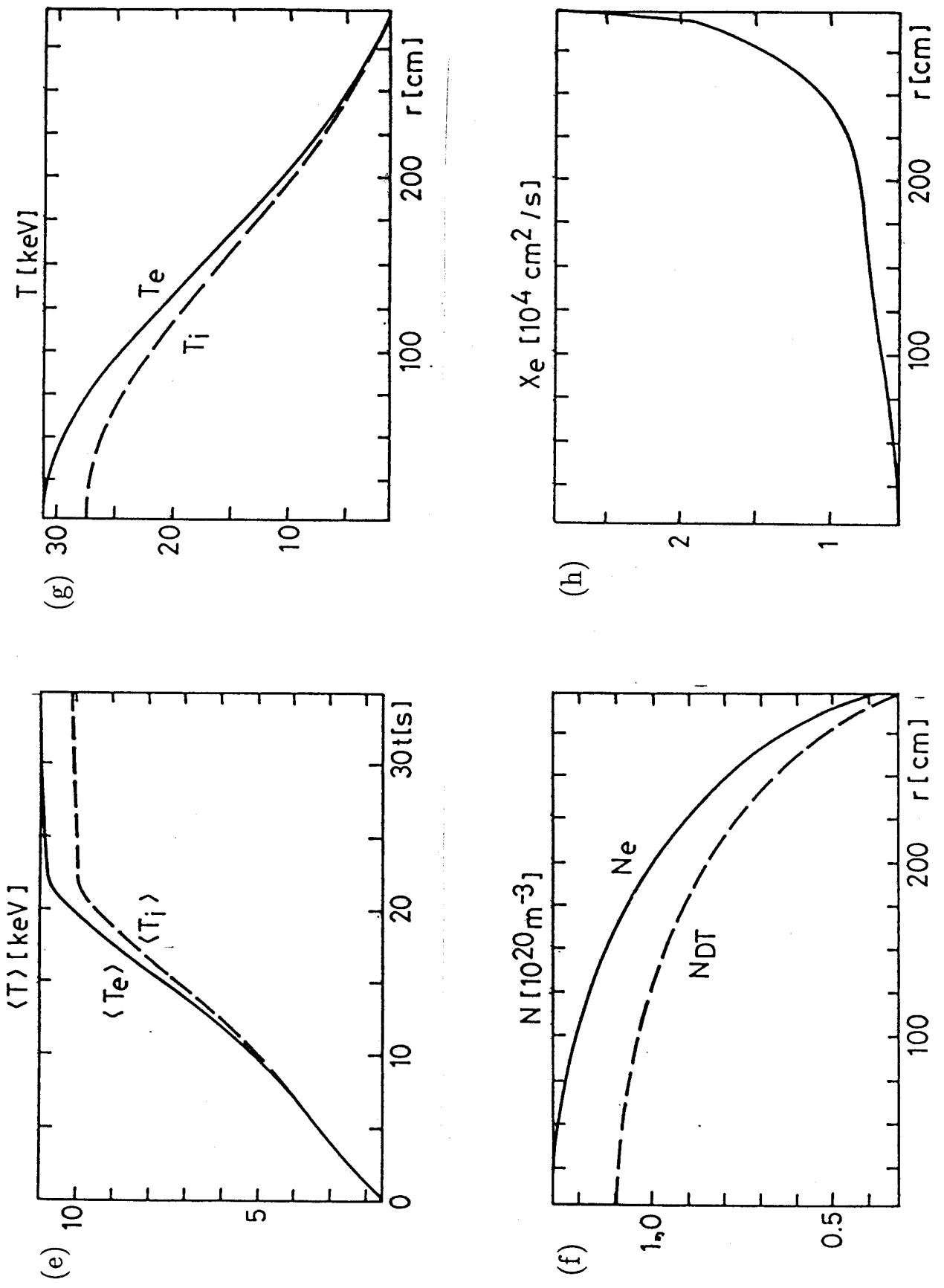
(e)
⟨T⟩ [keV]
⟨Te⟩
⟨Ti⟩
10
5
0
10
20
30t[s]
(f)
N [10^20 m^-3]
Ne
NDT
1,0
0.5
100
200
r [cm]
(g)
T [keV]
Te
Ti
30
20
10
100
200
r [cm]
(h)
Xe [10^4 cm^2/s]
2
1
100
200
r [cm]

Figure 7

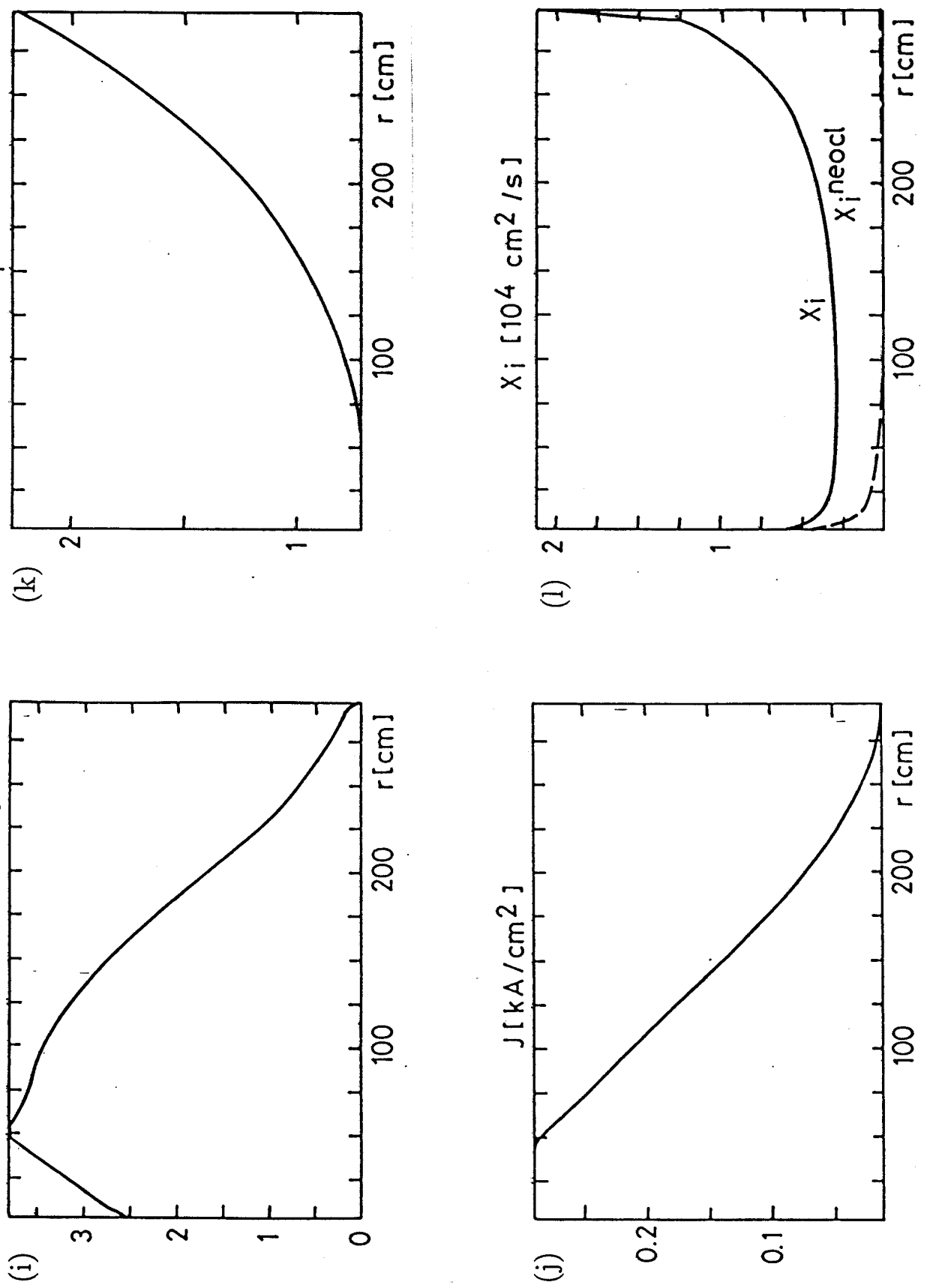
(i)
Pohm [10^-3 W/cm^3]
r [cm]
(j)
J [kA/cm^2]
r [cm]
(k)
q
r [cm]
(l)
χi [10^4 cm^2/s]
χi
χi^neocl
r [cm]

Figure 8

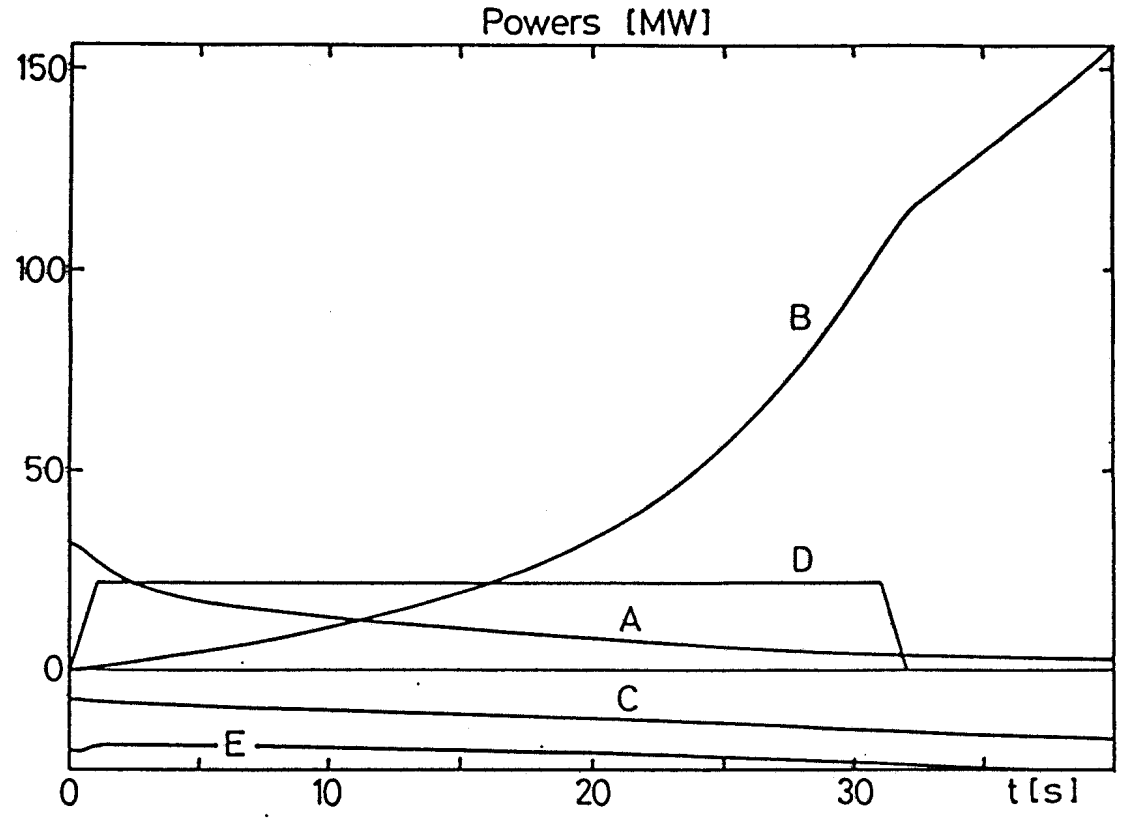

Figure 9

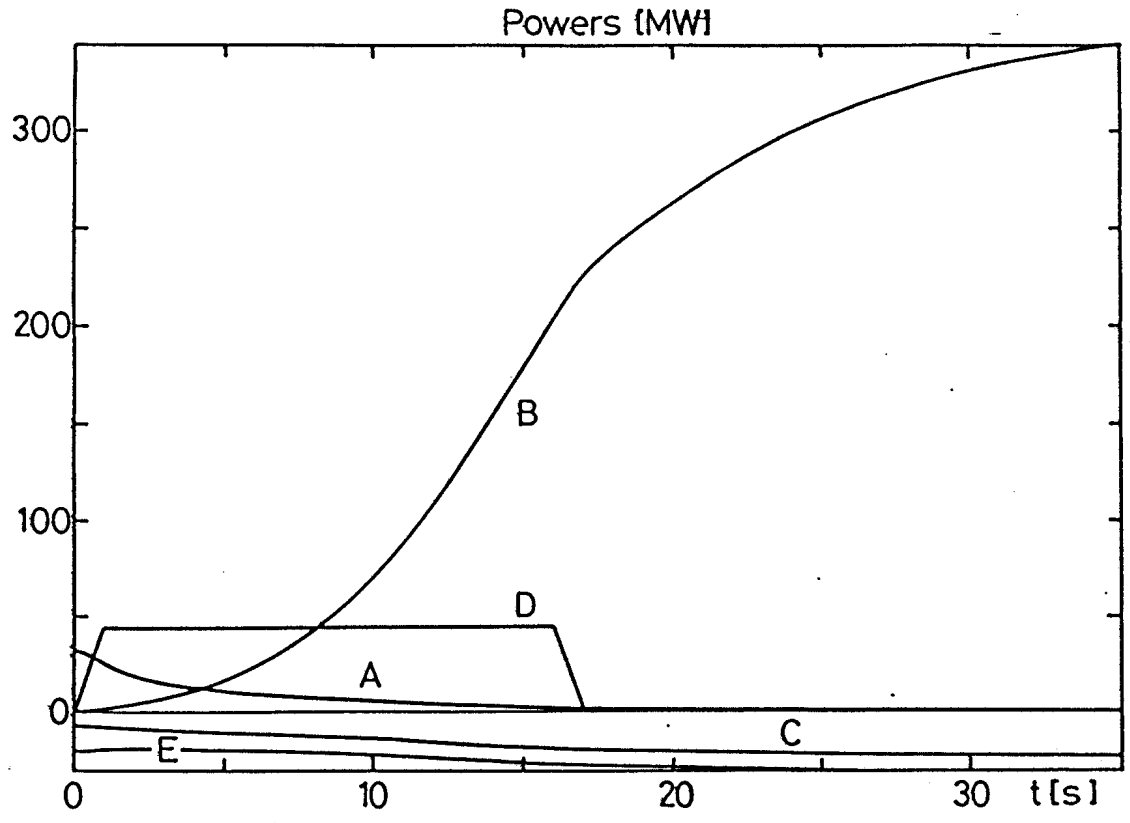

Figure 10

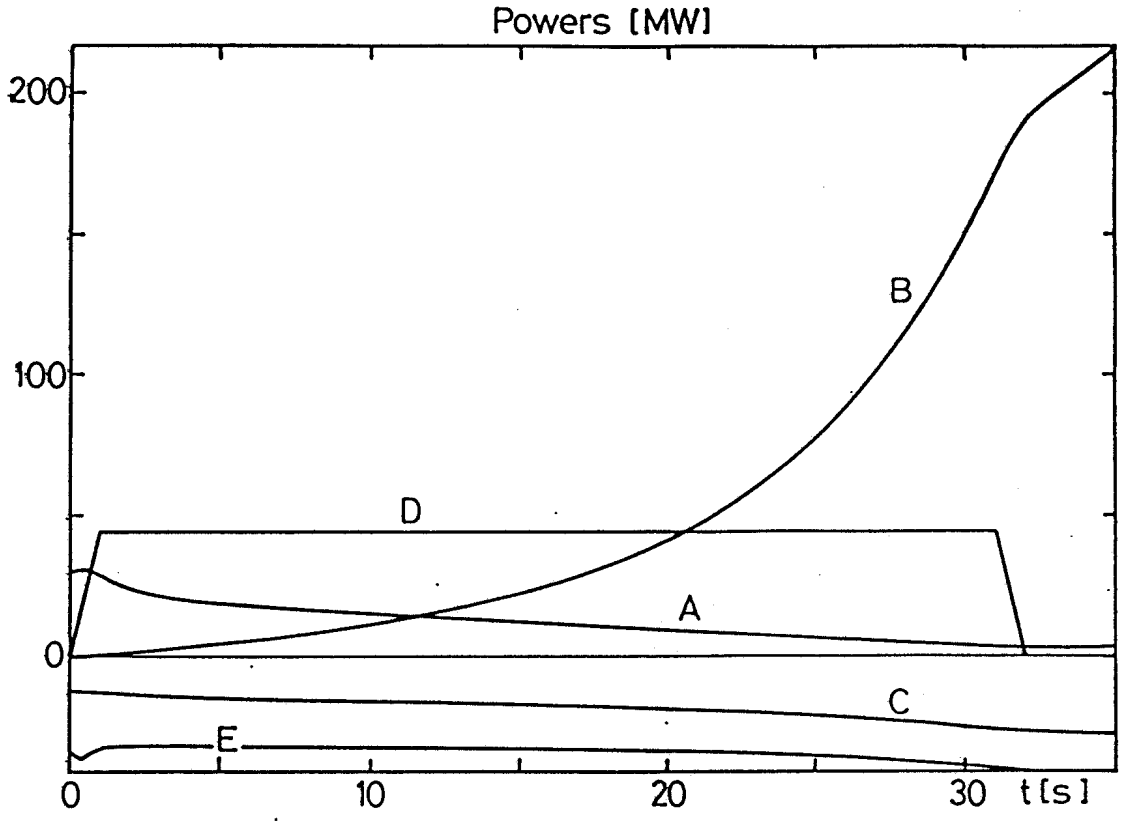

Figure 11

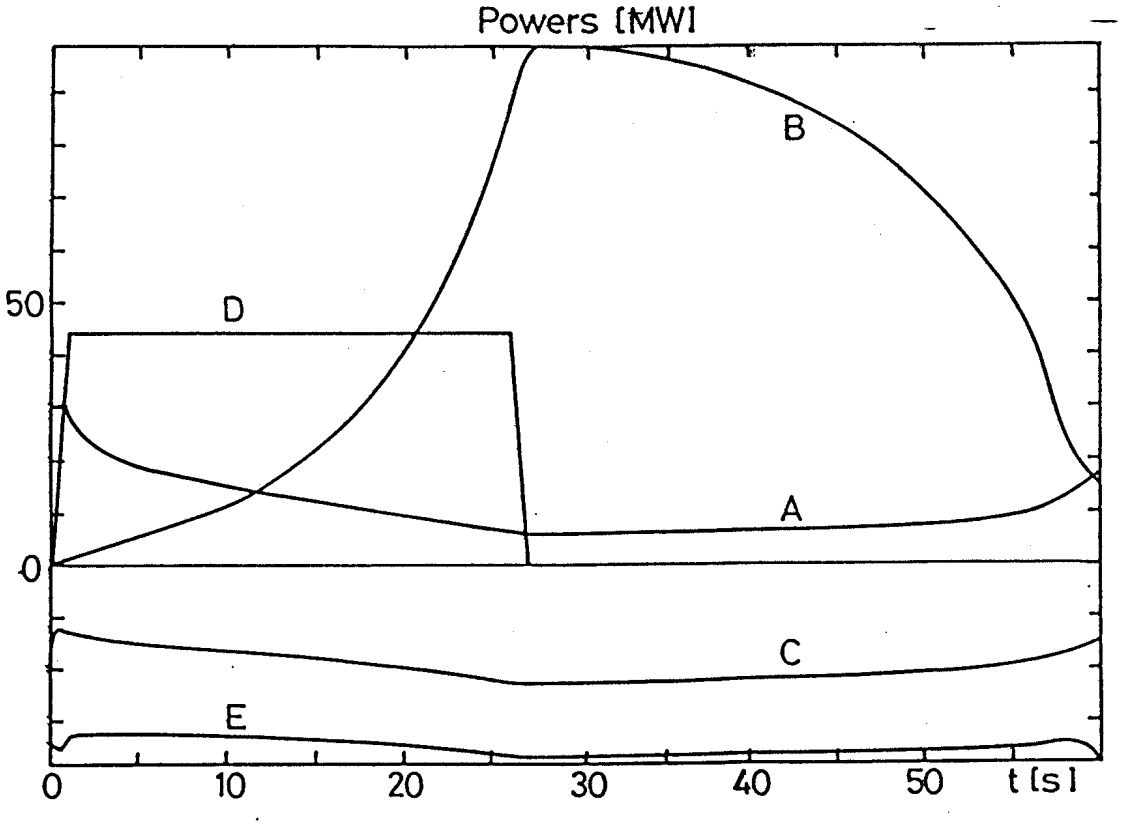

Figure 12

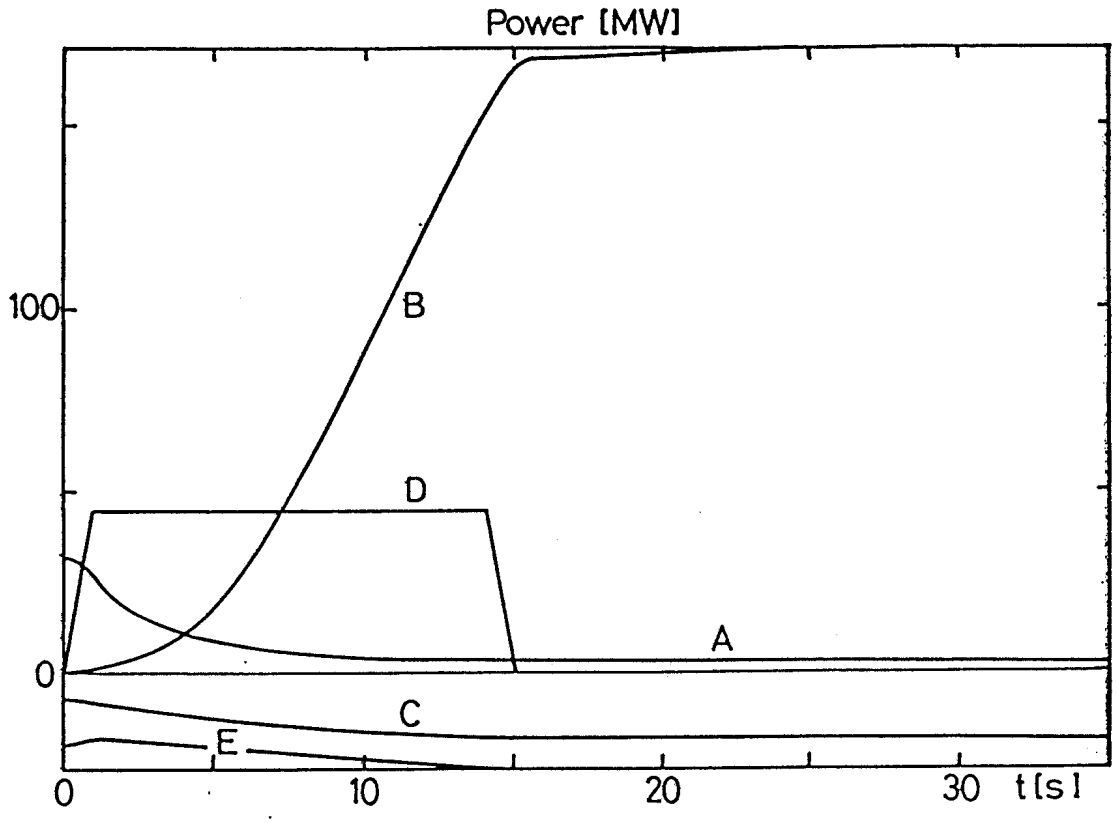

Figure 13

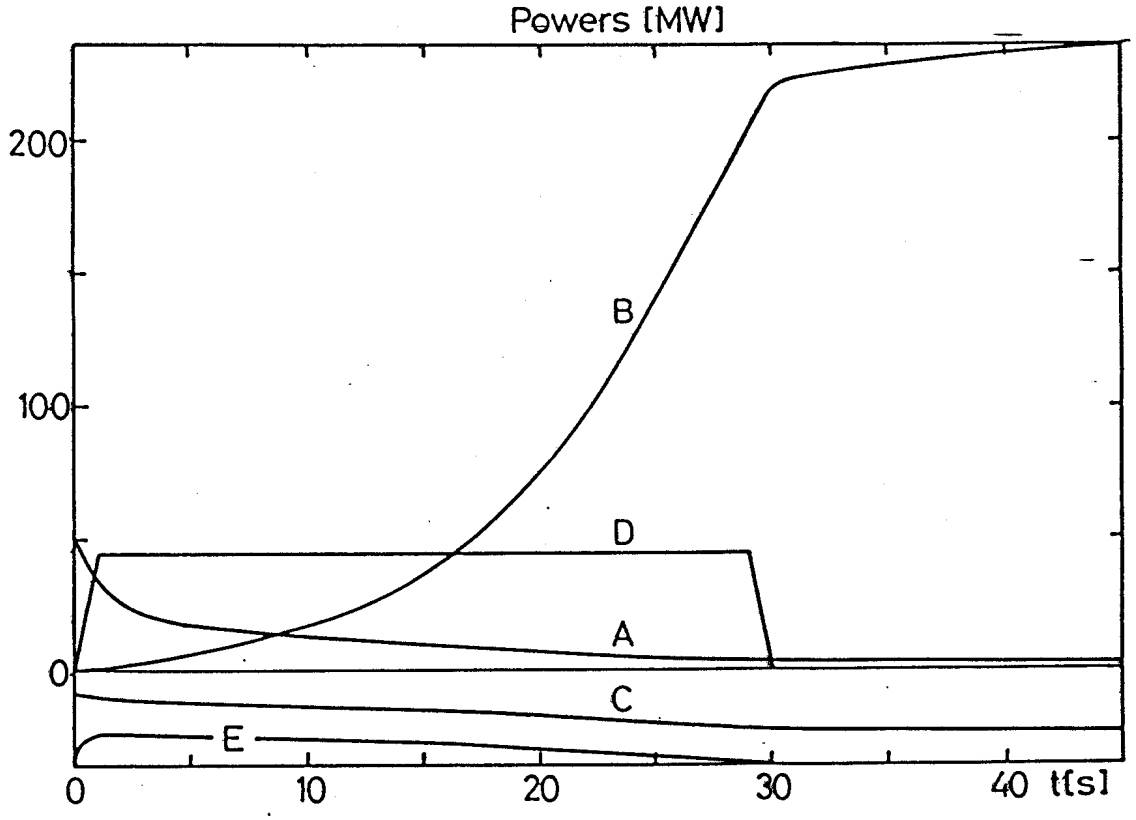

Figure 14

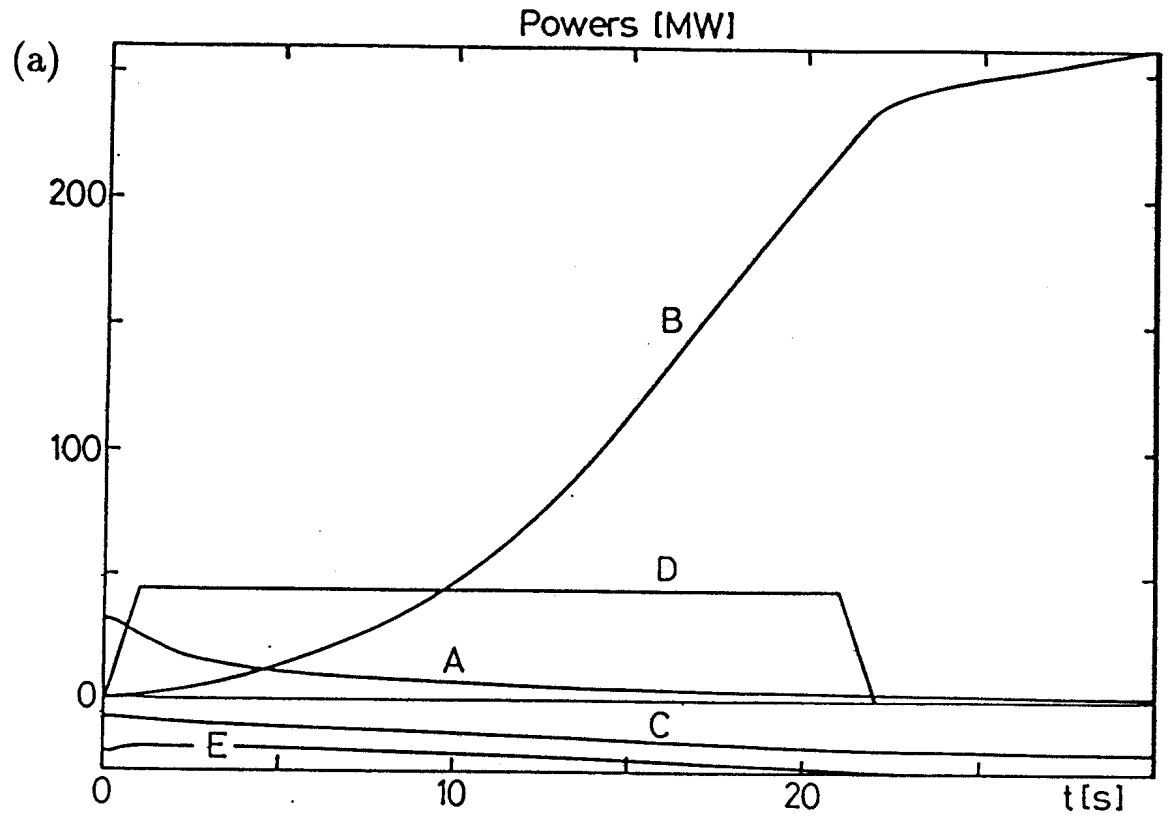
(a)
Powers [MW]
200
100
0
B
D
A
C
E
0
10
20
t [s]

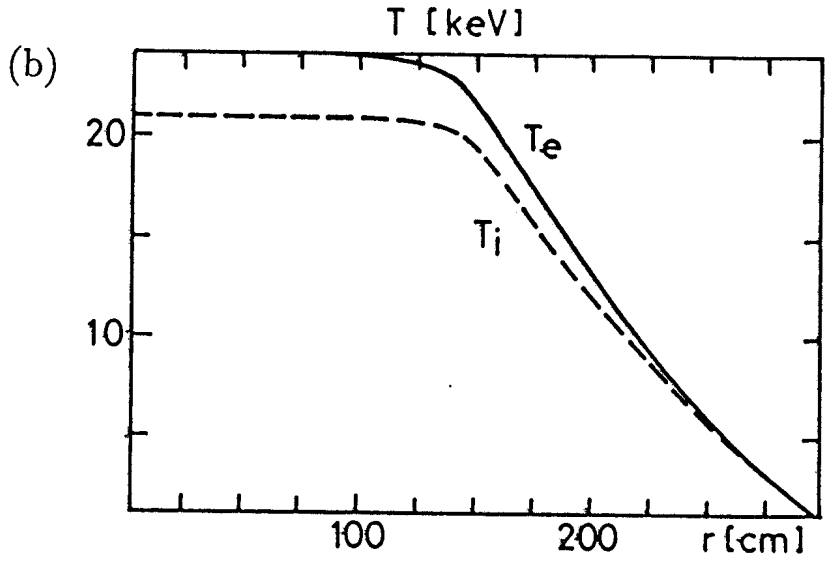
(b)
T [keV]
20
10
Te
Ti
100
200
r [cm]

Figure 15

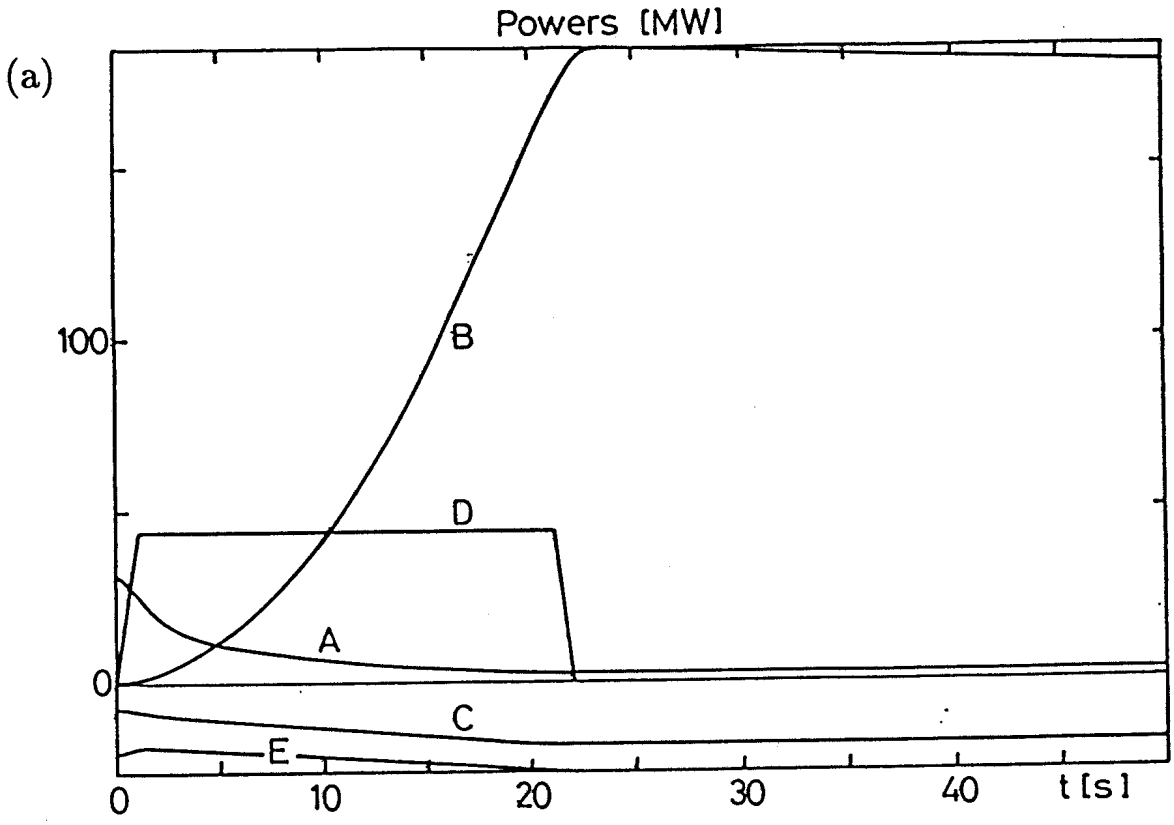
(a)
Powers [MW]
100
0
B
D
A
C
E
0
10
20
30
40
t [s]

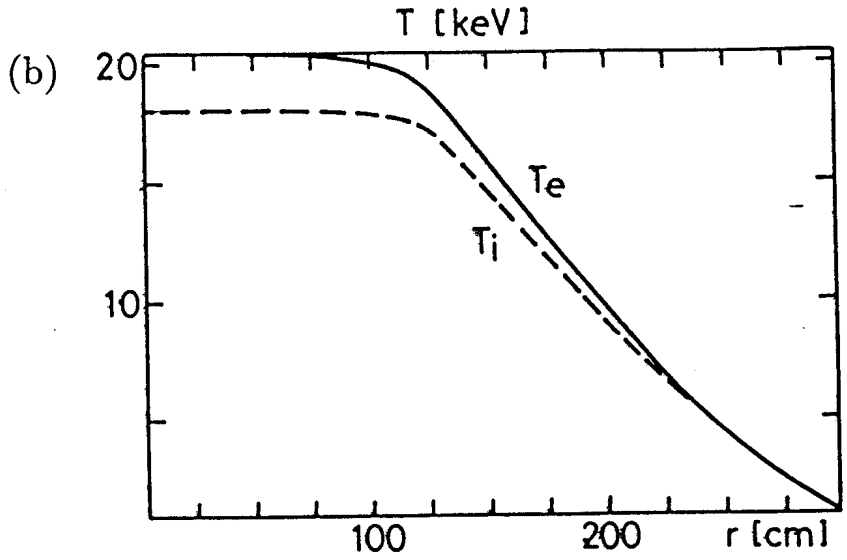
(b)
T [keV]
20
10
Te
Ti
100
200
r [cm]

Figure 16

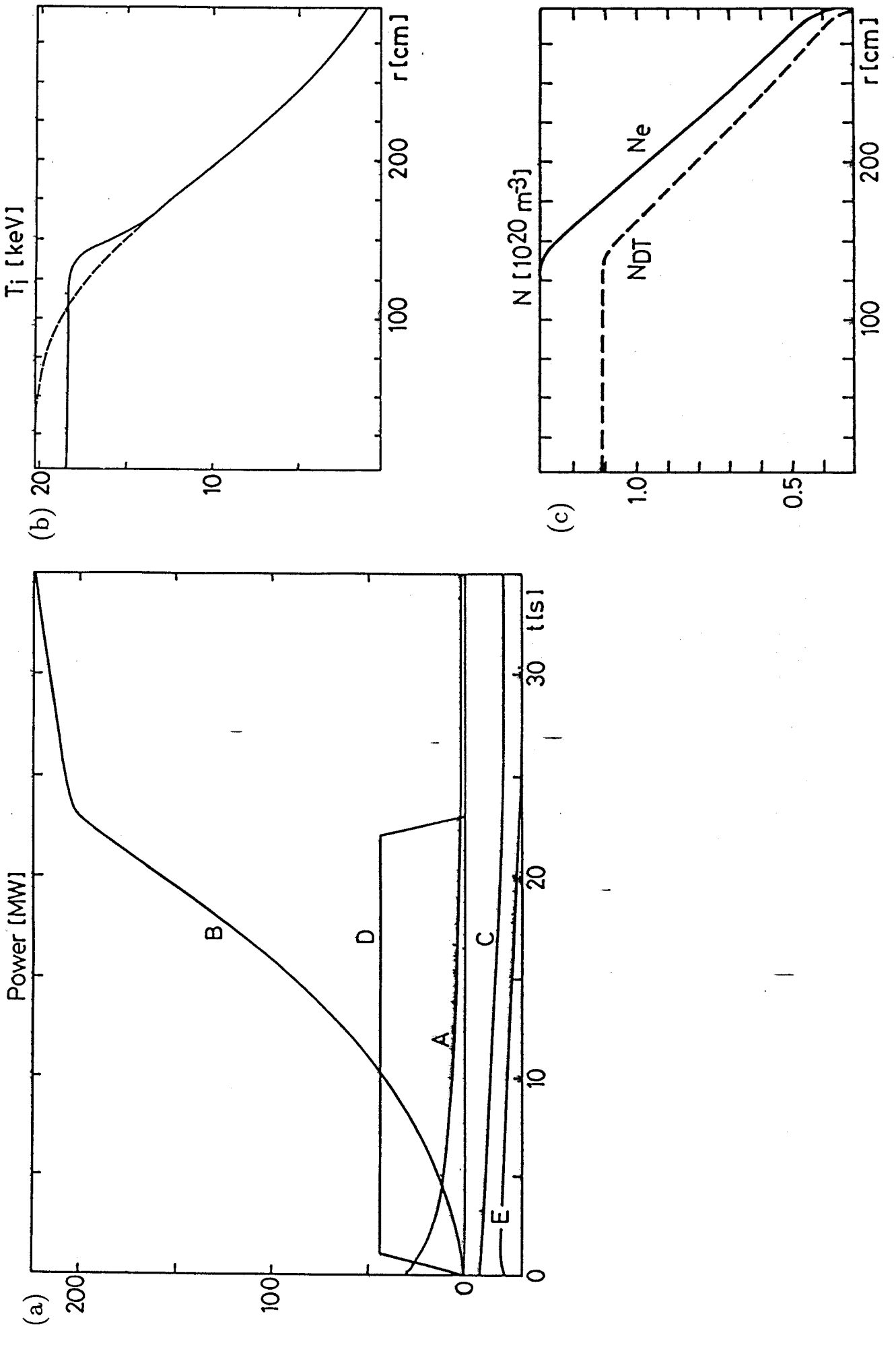
(a)
Power [MW]
200
100
0
0
10
20
30
t [s]
A
B
C
D
E
(b)
T_i [keV]
20
10
100
200
r [cm]
(c)
N [10^{20} m^{-3}]
1.0
0.5
100
200
r [cm]
Ne
N_{DT}